UNIVERSIDADE D
COIMBRA

António Manuel Aragão Aresta Valinho de Figueiredo

PREPARATION OF NFC-BASED FILMS WITH INCORPORATED MINERALS

FOR PACKAGING AND PRINTED ELECTRONICS USES

Master Thesis in Chemical Engineering supervised by Doctor José Gamelas and Doctor Paulo Ferreira, submitted to the Department of Chemical Engineering of the Faculty of Science and Technology of University of Coimbra

Coimbra, October 2020

António Manuel Aragão Aresta Valinho de Figueiredo

PREPARATION OF NFC-BASED FILMS WITH INCORPORATED MINERALS

FOR PACKAGING AND PRINTED ELECTRONICS USES

Dissertation submitted to the Department of Engineering of the Faculty of Science and Technology of University of Coimbra

Supervisors

Doctor José António Ferreira Gamelas

Doctor Paulo Jorge Tavares Ferreira

Coimbra, October 2020

UNIVERSIDADE D COIMBRA

«Knowing is not enough – we must apply.
Willing is not enough – we must do»
(Johann Wolfgang von Goethe)

Acknowledgements

I would like to start by acknowledging Dr. José Gamelas, who made resources available and accompanied me with all his dedication and rigour, which challenged me to further prove myself and conclude this final stage of my route in University of Coimbra. I cannot forget Dr. Paulo Ferreira, who was always concerned about us and our work, through the rough semester this was. I extend this gratitude to Dr. Luís Alves, for his guidance throughout this project, either by sharing his knowledge with me, or by assisting me whenever I needed the help, that proved crucial to the development of this work.

I also acknowledge Ricardo Almeida, for the essential support he provided me during inverse gas chromatography. This extends to all those working in B28 and B29, that were always available to assist me whenever I was in the need of help.

I would also like to thank Dra. Carla Vitorino, who provided us the laboratory and support at Faculty of Pharmacy, where the mechanical tests were performed.

My acknowledgement extends to all my friends who were with me since day one, with a special note to Bruno Alves, Filipa Simão, Beatriz Sampaio and Cristiana Bento, for the company during ours breaks, that made this unusual semester more bearable.

A very special thank goes to Carolina, for the patience and support I was given throughout the years, which undoubtedly made and still makes things better.

Lastly, but not least, a profound acknowledgement is given to my family, especially my parents, Manuela and Alexandre, who made everything possible for me to be here. If not for them, nothing of this would be done, and all I can do is thank them and conclude this stage of my life.

Abstract

Over the years, more ecological and sustainable alternatives are being pursued to replace plastics and other pollutant sources. Cellulose, being a renewable resource, becomes a good replacement option, especially when nanocelluloses are exploited, due to their excellent properties. The purpose of this dissertation is finding suitable alternatives for the use of plastics, using nanofibrillated celluloses (NFC), obtained from different pre-treatments of bleached eucalyptus pulp, and fibrous clays (sepiolite and palygorskite), to produce films with improved mechanical and gas barrier properties, while maintaining the high transparency to light associated with NFCs.

This work was divided in two main stages: i) inverse gas chromatography (IGC) studies, to assess the physicochemical properties of the materials' surfaces (NFC and minerals) and ii) preparation of NFC-based films. NFCs obtained from three distinct pre-treatments were used (mechanical, enzymatic or chemical (TEMPO-mediated oxidation)), and different quantities of minerals were incorporated in the films (0%, 10% and 50%). To prepare these films, solvent casting and vacuum filtration were the chosen techniques, and for the latter, two drying methods. Elongation at break tests were performed, as well as the measurement of the thickness and light transmittance of the films.

The dispersive component of the surface energy (γ^{sd}) followed a decreasing trend when increasing the temperature, in the range of 35 to 50ºC, having been obtained γ^{sd} values from 32 to 49 $mJ.m^{-2}$, with the mechanical pre-treated NFC exhibiting the highest value for γ^{sd} (48.9 $mJ.m^{-2}$ at 35ºC). By injecting polar probes, the prevalent Lewis acidic character of the NFC samples was verified. The specific components of the enthalpy and entropy of adsorption of polar probes were not considered due to poor correlation coefficients. Minerals' surface was also evaluated, with γ^{sd} values of 115.9 and 83.4 $mJ.m^2$, at 240ºC, for sepiolite and palygorskite, respectively.

Films without incorporated minerals were transparent. Even with 10% mineral, some films were still transparent, especially those from chemically pre-treated NFCs (TEMPO-oxidized NFCs). In fact, promising results for light transmittance (LT) were attained with 10% of mineral for TEMPO-oxidized NFCs: 19.6 and 30.2% for NFC TEMPO 110 and 165, respectively. Increasing the mineral content to 50% led to a massive increase in opacity. Films obtained by filtration exhibited higher thicknesses,

which led to a lower transparency observed in these films. Regarding mechanical properties, the latter films yielded the best results, by resisting to tensile strengths up to 83.9 MPa for pure NFC films, and up to 77.4 MPa was achieved for NFC films with 10% of mineral.

This work produced promising results regarding the preparation of hybrid organic-inorganic composite films. The results of this dissertation could be further improved by using new approaches, such as membrane filtration, or by altering the pH conditions, in order to obtain films with better properties.

Keywords: Nanofibrillar Cellulose, Sepiolite, Palygorskite, Inverse Gas Chromatography, Solvent Casting, Vacuum Filtration, Films.

Resumo

Ao longo dos anos, alternativas mais ecológicas e sustentáveis têm vindo a ser procuradas com o objetivo de substituir plásticos e outros materiais que poderão ser fonte de poluição. Sendo a celulose um recurso renovável, esta apresenta-se como uma boa opção, especialmente quando exploradas as nanoceluloses, dadas as suas excelentes propriedades. O objetivo da presente dissertação é a identificação de alternativas adequadas ao uso dos plásticos, recorrendo a celuloses nanofibriladas (NFC), obtidas por diferentes tratamentos de pasta branqueada de eucalipto, e minerais (paligorsquite e sepiolite), para produzir filmes com melhores propriedades mecânicas e de barreira à passagem de gases, mantendo, ao mesmo atempo, a elevada transparência à luz associada às NFCs.

Este trabalho foi dividido em duas etapas principais: i) estudos por cromatografia gasosa inversa (IGC) para avaliar as propriedades físico-químicas da superfície dos materiais (NFC e minerais), e ii) preparação de filmes à base de NFCs. Usaram-se NFCs obtidas por três tipos distintos de pré-tratamento (mecânico, enzimático ou químico (oxidação mediada pelo radical TEMPO)), e diferentes quantidades de minerais foram incorporadas nos filmes (0%, 10% e 50%). Para preparar os filmes, utilizaram-se técnicas de evaporação de solvente e de filtração a vácuo e, para a última, dois métodos de secagem. Realizaram-se ensaios de tração, tendo-se ainda medido a espessura e a transmitância à luz dos filmes.

A componente dispersiva da energia de superfície (γ^{sd}) seguiu uma tendência decrescente, com o aumento da temperatura, na gama de 35-50ºC, tendo-se obtido valores desde 32 a 49 $mJ.m^{-2}$, sendo a NFC mecânica a que exibiu o maior valor de γ^{sd} (48.9 $mJ.m^{-2}$, a 35ºC). Ao injetar provas polares, verificou-se a prevalência do carácter ácido de Lewis de todas as NFCs. As componentes específicas da entalpia e entropia de adsorção das provas polares não foram consideradas devido aos baixos coeficientes de correlação. A superfície dos minerais foi também avaliada, obtendo-se valores para γ^{sd}, a 240ºC, de 115.9 e 83.4 $mJ.m^{-2}$ para a sepiolite e paligorsquite, respetivamente.

Os filmes sem minerais incorporados evidenciaram-se transparentes, sendo possível ver através dos mesmos. Mesmo quando utilizado 10% de mineral, alguns filmes mantiveram-se transparentes, especialmente aqueles obtidos a partir de NFC quimicamente pré tratada (NFCs oxidadas com TEMPO). Efetivamente, foram obtidos

resultados promissores para a transmitância no visível (LT) com 10% de mineral para NFCs oxidadas com TEMPO: valores de LT de 19.6% e 30.2% para NFC TEMPO 110 e NFC TEMPO 165, respetivamente. Filmes com 50% de mineral resultaram num aumento significativo da opacidade. A filtração a vácuo levou a filmes com maior espessura, o que se traduziu numa menor transparência observada nestes filmes. Relativamente às propriedades mecânicas, os filmes preparados através da filtração originaram os melhores resultados, resistindo a tensões até 83.9 MPa para filmes apenas com NFC, e até 77.4 MPa para filmes de NFC com com 10% de mineral.

O presente trabalho proporcionou resultados promissores relativamente à preparação de filmes compósitos híbridos orgânico-inorgânico, podendo os mesmos ser melhorados através de técnicas como a filtração por membranas, ou alterando as condições de pH, para procurar obter filmes com melhores propriedades.

Palavras-chave: Celulose Nanofibrilar, Sepiolite, Paligorsquite, Cromatografia Gasosa Inversa, Evaporação de Solvente, Filtração a Vácuo, Filmes.

Table of Contents

List of Figures iii

List of Tables vi

Nomenclature viii

1. Introduction 1

1.1. Motivation 1

1.2. Structure of the Thesis 3

2. State of the Art 5

2.1. Nanofibrillar Cellulose 5

2.2. Fibrous Clay Minerals 9

2.2.1. Palygorskite and Sepiolite 11

2.3. Hybrid organic-inorganic composite films 14

2.4. Film Preparation Methods 18

2.5. Inverse Gas Chromatography (IGC) 19

2.5.1. IGC relevance in film preparation 24

3. Materials and Methods 25

3.1. NFC 25

3.2. Fibrous minerals 26

3.3. Inverse Gas Chromatography (IGC) 26

3.4. X-Ray diffraction analysis 28

3.5. NFC and Composite Films 28

3.5.1. Solvent Casting 28

3.5.2. Vacuum Filtration 30

3.6. Films testing 31

4. Results and Discussion 33

4.1. Inverse Gas Chromatography (IGC) 33

4.1.1 Dispersive component of the surface energy (γ^{sd}) 35

4.1.2. Lewis acid-base character 38

4.1.3. Specific component of enthalpy (ΔH^s) and entropy (ΔS^s) 41
4.1.4. Sepiolite and Palygorskite IGC Analysis 43
4.2. NFC-based films 44
5. Conclusions 63
6. Future Prospects 67
7. Bibliography 68

List of Figures

Figure 1. Summarized pathways for the obtention of the different cellulose types (Adapted from Wei et al., 2014)……5

Figure 2. Representative scheme of NFC obtention (Adapted from Alves et al., 2019)……..7

Figure 3. The basic structure of phyllosilicates (Nelson, 2015)……..9

Figure 4. Structure of palygorskite (attapulgite) and sepiolite (Millot, 1970)……12

Figure 5. Schematic comparison between GC and IGC (Adapted from Milczewska and Voelkel, 2012)……19

Figure 6. Example of a linear fit of RT.ln(VN) as a function of 2N.a.√γld……21

Figure 7. Example of a linear fit of ΔG/T as a function of 1/T……..…….22

Figure 8. Example of a chromatogram, for methane……...28

Figure 9. Filtration setup, consisting of two Kitasato flasks, a vacuum pump and a filter plaque with a porosity of 45µm……...30

Figure 10. Schematic representation of elongation at break test……..…31

Figure 11. Dispersive component of surface energy for all NFC samples at 35ºC…..…36

Figure 12. Dispersive component of surface energy ($mJ.m^{-2}$) as a function of temperature (ºC), for all samples…….…….37

Figure 13a. Specific works of adhesion for NFC Mec, in $mJ.m^{-2}$……38

Figure 13b. Specific works of adhesion for NFC TEMPO 55, in $mJ.m^{-2}$……38

Figure 13c. Specific works of adhesion for NFC TEMPO 165, in $mJ.m^{-2}$……...39

Figure 13d. Specific works of adhesion, for NFC – E1, in $mJ.m^{-2}$…….…39

Figure 13e. Specific works of adhesion, for NFC – E2, in $mJ.m^{-2}$……..39

Figure 14a. ΔG^{as} as a function of 1/T for DCM for NFC Mec……42

Figure 14b. ΔG^{as} as a function of 1/T for THF for NFC Mec……42

Figure 14c. ΔG^{as} as a function of 1/T for ETA for NFC Mec……43

Figure 15a. Composite films for NFC Mec with 0% mineral (bottom), 10% mineral (middle) and 50% mineral (top), produced through solvent casting……45

Figure 15b. Composite films for NFC-E1 with 0% mineral (bottom), 10% mineral (middle) and 50% mineral (top), produced through solvent casting……45

Figure 15c. Composite films for NFC TEMPO 55 with 0% mineral (bottom), 10% mineral (middle) and 50% mineral (top), produced through solvent casting……..46

Figure 15d. Composite films for NFC TEMPO 110 with 0% mineral (bottom), 10% mineral (middle) and 50% mineral (top), produced through solvent casting…..……..46

Figure 15e. Composite films for NFC TEMPO 165 with 0% mineral (bottom), 10% mineral (middle) and 50% mineral (top), produced through solvent casting……..47

Figure 16a. NFC only films, for all NFC samples (from left to right: NFC Mec, NFC-E1, NFC TEMPO 55, NFC TEMPO 110 and NFC TEMPO 165)……48

Figure 16b. Films with 10% PAL, for all NFC samples (from left to right: NFC Mec, NFC-E1, NFC TEMPO 55, NFC TEMPO 110 and NFC TEMPO 165)……..49

Figure 16c. Films with 10% SEP, for all NFC samples (from left to right: NFC Mec, NFC-E1, NFC TEMPO 55, NFC TEMPO 110 and NFC TEMPO 165)…….49

Figure 16d. Films with 50% PAL, for all NFC samples (from left to right: NFC Mec, NFC-E1, NFC TEMPO 55, NFC TEMPO 110 and NFC TEMPO 165)…….49

Figure 16e. Films with 50% SEP, for all NFC samples (from left to right: NFC Mec, NFC-E1, NFC TEMPO 55, NFC TEMPO 110 and NFC TEMPO 165)…….50

Figure 17a. Films obtained through vacuum filtration (F) and dried at room temperature (1) and in the oven at 50ºC (2), for NFC Mec……51

Figure 17b. Films obtained through vacuum filtration (F) and dried at room temperature (1) and in the oven at 50ºC (2), for NFC-E1……..51

Figure 17c. Films obtained through vacuum filtration (F) and dried at room temperature (1) and at an oven at 50ºC (2), for NFC TEMPO 55, 110 and 165…….51

Figure 18. Microscope image of the cross-section of a NFC film for thickness measurement (NFC TEMPO 55), obtained through solvent casting…….52

Figure 19. Operating conditions used on the elongation at break test, set on the testing software……...57

List of Tables

Table 1. Comparison between results obtained for mechanical properties by Wu *et al.*, 2012 and Wu *et al.*, 2014, using TEMPO-oxidized NFC with MTM and SS……15

Table 2. Consistency of the prepared NFC samples, in percentage (w/w %)……..…….26

Table 3a. Quantities of NFC and mineral suspensions needed to prepare films with 10% mineral (dry weight)……..……29

Table 3b. Quantities of NFC and mineral suspensions needed to prepare films with 50% mineral (dry weight)……..……29

Table 4. Operating conditions of IGC analysis…….……..33

Table 5. Retention times for all probes and NFC sample, at 35ºC, in seconds (s)…….34

Table 6. Dispersive component of the surface energy (γ^{sd}) obtained for the different NFC samples, in $mJ.m^{-2}$……35

Table 7. Crystallinity of the NFC samples determined through X-ray diffraction…….37

Table 8. Ratio between the specific work of adhesion of THF and TCM, at different temperatures……..……40

Table 9. Ratio between the specific work of adhesion of ethyl ether and TCM, at different temperatures…….40

Table 10. Specific enthalpy and entropy obtained for TEMPO 165, with and without values at 45ºC……...41

Table 11. Specific component of enthalpy and entropy obtained from DCM, THF and ETA, for NFC Mec……...43

Table 12. Dispersive component of surface energy (γ^{sd}) for sepiolite (SEP) and palygorskite (PAL) samples…….44

Table 13. Average thickness, in μm, for the films obtained through solvent casting…..53

Table 14a. Average thickness, in μm, for the films obtained through vacuum filtration, and dried at room temperature……..53

Table 14b. Average thickness, in μm, for the films obtained through vacuum filtration, and dried at an oven at 50ºC……..54

Table 15a. Light transmittance, in %, for films obtained through solvent casting……..54

Table 15b. Light transmittance, in %, for films obtained through vacuum filtration and dried at room temperature (Batch 1) and in theoven at 50ºC (Batch 2)……55

Table 16a. Load force (N) and stretched distance (mm) before failure, for films obtained through solvent casting……57

Table 16b. Load force (N) and stretching distance (mm) before failure, for films obtained through vacuum filtration and dried at room temperature (Batch 1) and in the oven at 50ºC (Batch 2)……..59

Table 17a. Tensile strength (MPa), elongation at break (%) and Young's modulus (GPa), for films obtained through solvent casting……..59

Table 17b. Tensile strength (MPa), elongation at break (%), and Young's modulus for films obtained through vacuum filtration and dried at room temperature (Batch 1) and in the oven at 50ºC (Batch 2)……60

Nomenclature

A – Area of the cross-section

a – Probe's molecular area

AcR – Acrylic resin

AR – Aspect ratio

ATT – Attapulgite

CAE – Cation exchange capacity

DCM – Dichloromethane

E – Young's modulus

E1 – Enzyme 1

E2 – Enzyme 2

ETA – Ethyl Acetate

F – Applied load force

GC – Gas chromatography

HNFC – High-charged density nanofibrillar celulose

I_{002} – Maximum intensity of the (002) lattice diffraction

I_{am} – Intensity of diffraction at $2\theta=18^{o}$

IGC – Inverse gas chromatography

I_M – Nanomorphological index

I_{sp} – Specific component of the surface energy

J – James-Martin correction factor

L0 – Original distance between the grips

LT – Light transmittance

MNFC – Medium-charged density nanofibrillar cellulose

MTM – Montmorillonite

N – Avogadro's number

NCA – Nanocellulose attapulgite composite

NCC – Nanocrystalline gellulose

NFC – Nanofibrillar cellulose

OTR – Oxygen transfer rate

P – Absolute pressure of operation

PAL - Palygorskite

PE – Polyamidoamine epichlorohydrin

P-NFC – Phosphorylated nanofibrillar cellulose

PP – Polypropylene

R – Ideal gas constant

SEP – Sepiolite

T – Temperature

t_0 – Retention time of the reference probe

TCM – Trichloromethane

THF – Tetrahydrofuran

t_r – Retention time of the injected probe

VN – Net retention volume

W^{as} – Work of adhesion

γ^{ld} – Dispersive component of the probe's surface energy

γ^{sd} – Dispersive component of the solid's surface energy

ΔG^{as} – Free energy of adsorption

ΔH^{as} – Specific component of the enthalpy

ΔL – Change in the film's length

ΔS^{as} – Specific component of the entropy

1. Introduction

1.1. Motivation

Over the past years, there has been an increased interest in reducing the use of conventional plastics, due to the problems associated with its production, recycling, or elimination. In order to find suitable substitutes, some eco-friendly alternatives are being studied, with a special interest in materials produced from vegetable and mineral resources. Nanocelluloses exhibit remarkable mechanical properties, while minerals show very good gas barrier properties, making hybrid organic-inorganic composites an interesting approach to solving the plastics problem.

The main purpose of the present work is the preparation of hybrid composite films, with nanofibrillated cellulose (NFC) as the matrix, and fibrous nanoclays as filler. This combination aims not only to obtain films with good mechanical properties, but also intends to decrease the oxygen and water vapor permeability, which are requirements for both packaging and printed electronic purposes.

NFCs are cellulose fibres at the nanometric scale, that constitute a good alternative to plastics, since they are renewable and biodegradable. Another positive aspect regarding the use of cellulose is the fact that the paper and pulp is a well-established industry in Portugal, allowing easier access to the raw materials to prepare the NFC. Cellulose nanofibrils-based films are known for its excellent mechanical properties (high Young's modulus and tensile strength) and good thermal stability, due to its low thermal expansion coefficient. Regarding gas barrier properties, NFC films also exhibit interesting properties, induced by its packed structure, which increases tortuosity and reduces the passage of gases through the films, such as oxygen and water vapor. However, due to the high hydrophilicity of NFCs, when subjected to high humidity environments, this barrier deteriorates. Thus, to overcome this limitation, as well as the high cost of NFC, the preparation of composites is suitable and appears as an interesting approach.

To prepare the composites, phyllosilicates were used as fillers in the present work, with special focus on fibrous clay minerals, such as palygorskite and sepiolite. In literature are reported different studies with the incorporation of planar minerals, such as montmorillonite and vermiculite, but very little attention was given on the use of fibrous minerals. These minerals resemble, in terms of morphology, to NFC (similar thickness

and length) and planar minerals (as they exhibit a layered chemical structure). Some important characteristics of fibrous minerals are their high surface area and porosity, making them very good adsorbents, and their cation exchange capacity (CAE). Besides the mentioned properties, there is also the fact that they exist in an abundant quantity in nature, becoming a very interesting opportunity. In fact, there is an increased interest in the incorporation of this category of minerals in an NFC matrix, which will allow the cost reduction of the hybrid composite films, keeping or improving the mechanical and barrier properties.

These films can be prepared using different approaches, such as solvent casting or vacuum filtration, among others. Each technique used, leads to different properties on the obtained film, hence the interest in finding out the most interesting and efficient film preparation method.

To anticipate the good compatibility between matrix and filler, the analysis of the surface properties of raw minerals and NFC by inverse gas chromatography (IGC) was performed.

1.2. Structure of the Thesis

The present thesis is divided in six (6) major Chapters:

- **Chapter 1**: Introduction

This Chapter includes the motivations of the work and the objectives of the study. Also includes the "Structure of the Thesis", mentioning the content of each Chapter.

- **Chapter 2**: State of the Art

This Chapter contains the current theoretical knowledge and previous experimental works in this field of research, considering the different approaches taken by other authors. It includes a literature review regarding nanofibrillated cellulose, clays, hybrid organic-inorganic composite films and inverse gas chromatography applied to clays and NFC.

- **Chapter 3**: Materials and Methods

The materials and methods used are explained in this Chapter, to allow the reproducibility of the experiment by other researchers. It includes information of the minerals, nanofibrillated cellulose, IGC methodology and composite films' preparation.

- **Chapter 4**: Results and Discussion

Results obtained on the main physical and mechanical properties of the hybrid composite films produced are presented and discussed in this Chapter. Results obtained from the IGC analysis, regarding NFC's surface characterization, are also presented.

- **Chapter 5**: Conclusions

This Chapter summarizes the conclusions inferred in the previous Chapter, also mentioning the difficulties encountered through the development of the work.

- **Chapter 6**: Future Prospects

Suggestions of work that would contribute to a better development of the present study and were not possible to perform in this thesis, are given in this Chapter.

- Annexes

Any data or complementary information considered important to deeply understand the present study is included in this Chapter.

2. State of the Art

2.1. Nanofibrillar Cellulose

The term nanocellulose is associated with nano-structured cellulose and includes three different categories: nanofibrillated cellulose (NFC), nanocrystalline cellulose (NCC) and bacterial cellulose. Overall, nanocelluloses are known by their large surface area, high tensile strength and stiffness, low density and thermal expansion coefficients (Alves *et al.*, 2019). A summarized pathway to obtain these types of nanocelluloses is given in **Figure 1**.

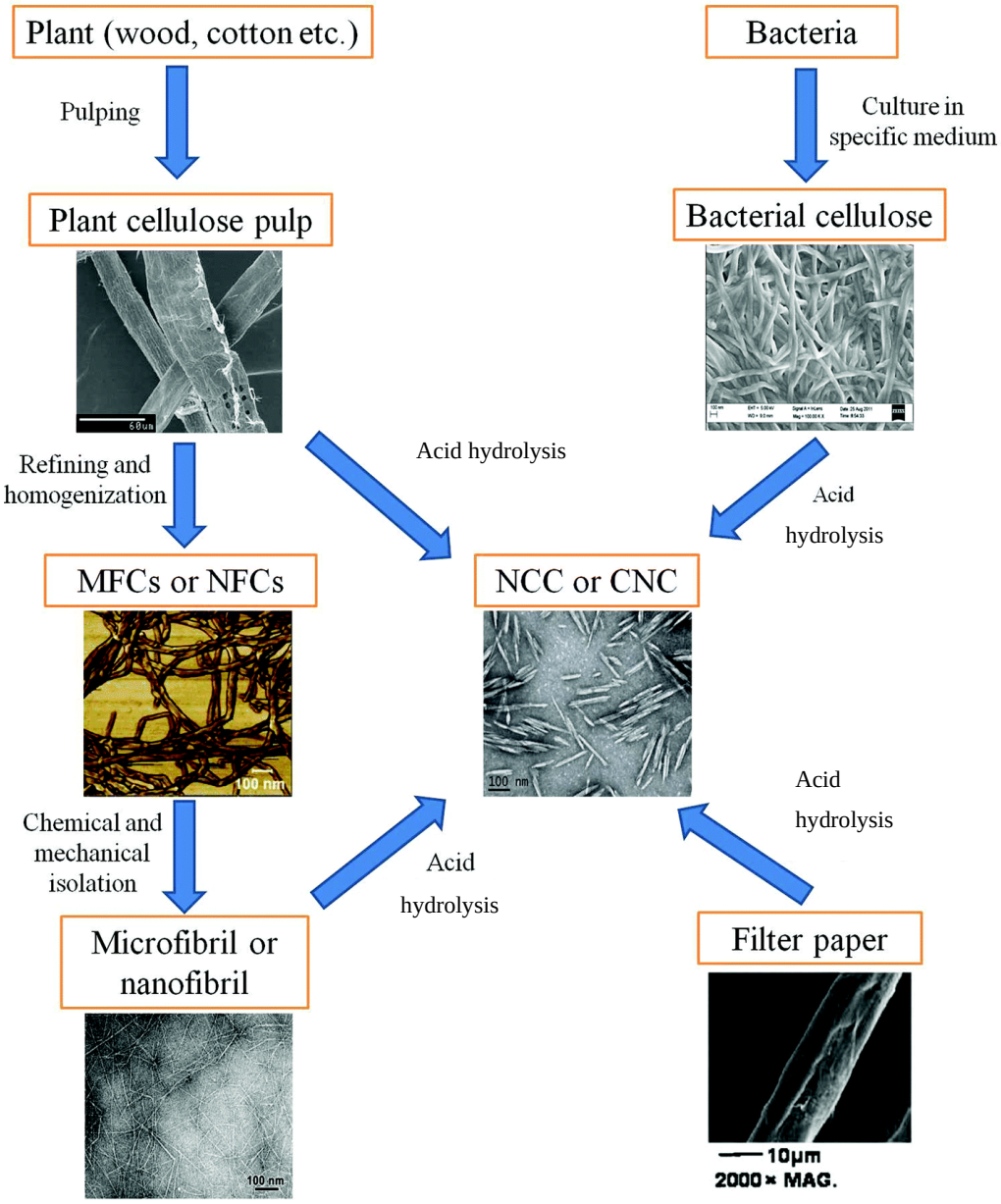

Figure 1. Summarized pathways for the obtention of the different cellulose types (Adapted from Wei et al., 2014).

Among them, there is a special interest in NFC, as it has higher surface area compared to regular cellulose fibres (up to over 100 m^2 g^{-1} difference) and exhibits extraordinary mechanical properties, with a tensile strength up to 180 MPa and Young's modulus up to 45 GPa (Wang *et al.*, 2015). They also exhibit other advantageous basic properties, such as their high availability as renewable materials, dimensional stability, biocompatibility and biodegradability (Eichhorn *et al.*, 2010). Due to these excellent properties, they have a wide range of applications, being used as a reinforcement material in composites (Benítez and Walther, 2017), for paper coating (Brodin *et al.*, 2018), as a barrier material for packaging and as a substrate for printed electronics (Alves *et al.* 2019; Gamelas and Ferraz, 2015; Fukuzumi *et al.*, 2008), among other uses. For example, the oxygen transfer rate (OTR) required for modified atmosphere packaging should be below 10 to 20 $mL.m^{-2}.day^{-1}$ whereas the OTR for nanocellulose films is from 4 to 18 $mL.m^{-2}.day^{-1}$, showing promising values for this type of application (Lavoine *et al.*, 2012).

NFC is a preferred choice rather than NCC or bacterial cellulose since its preparation is faster than bacterial cellulose's (Alves *et al. 2019*) and requires fewer chemicals than NCC's (Tibolla *et al.* 2016). However, NFC's main disadvantage lies on the high energy consumption during its mechanical processing and the heterogeneity of the resulting nanocellulose product (Yuan *et al.*, 2019), which can be minimized through several different pre-treatment approaches. Among the alternatives used to reduce energy consumption, the most used ones are enzymatic hydrolysis (Chen *et al.*, 2017; Tibolla *et al.*, 2016), TEMPO-mediated oxidation (Lourenço *et al.*, 2017; Isogai *et al.*, 2010) and carboxymethylation (Naderi *et al.*, 2015), but other options such as periodate oxidation (Errokh *et al.*, 2018; Liimatainen *et al.*, 2012;) and cationization (Rol *et al.*, 2019) are also used. Another challenge associated with NFC preparation and application is the low NFC content in the prepared suspensions and consequently the high drying or transport cost, (the resulting gels or suspensions can have up to 99% wt in water). The most commonly used methods are freeze and spray drying, which have a negative impact on the nanocellulose's properties, affecting crystallinity, leading to hornication (formation of irreversible agglomerates) and lowering thermal stability (Nelson *et al.*, 2016). The preparation of NFC is represented in **Figure 2** (Alves *et al.*, 2019).

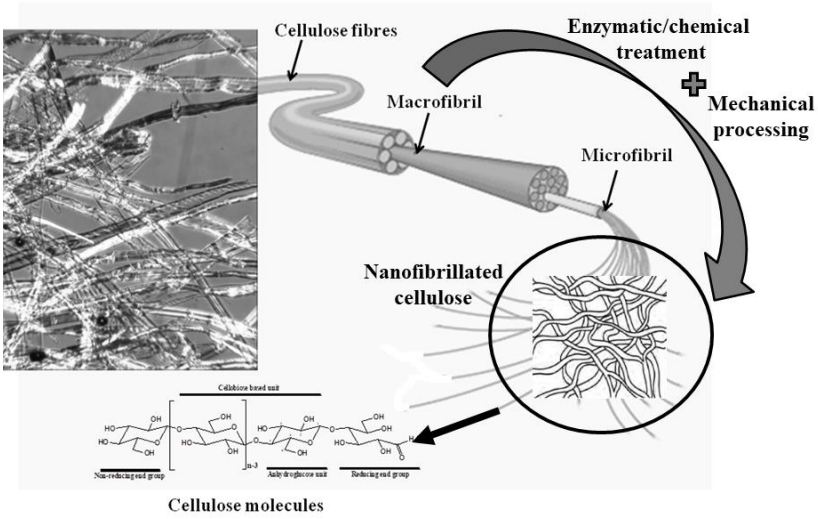

Figure 2. Representative scheme of NFC obtention (Adapted from Alves et al., 2019).

In terms of pre-treatment strategies, the enzymatic pre-treatment is often processed at mild conditions and has high selectivity. It is a very efficient method as it promotes peeling and fine fibrosis, which favours the fibrillation of the cellulose fibres in mechanical processing, thus reducing the energy consumption of these processes. It also appears as a good economical choice, since it reduces or even dismisses the need for solvents or chemicals. However, the nanofibrillation yield obtained by enzymatic pre-treatment is typically low, ca. 20%, using a low number of passes through the high-pressure homogenizer (Alves *et al.*, 2019; Cheng *et al.*, 2017).

On the other hand, the TEMPO-mediated oxidation approach is the most used one and consists in introducing negatively charged groups in the cellulose fibres, promoting delamination of the nanofibrils, due to electrostatic repulsion among negative charges (Alves *et al.*, 2019). This method allows the obtention of NFC films with excellent gas permeation selectivity, compared to non-pre-treated approaches, as those films exclusively adsorb positively charged species (Thielemans *et al.*, 2009). An NFC yield of around 90% on original pulp was reported by the USDA's Forest Products Laboratory when using sodium hypochlorite as the main oxidant. Their preparation method included several chemical and mechanical processes, leading to NFC with an estimated commercial cost of 196 €/kg (Nelson *et al.*, 2016).

Cellulose carboxymethylation is a pre-treatment to increase anionic charges by the formation of carboxyl groups, somehow similar to TEMPO-mediated oxidation, on the NFC's surface. Commonly, monochloroacetic acid is used as the modifying agent

(Lavoine *et al.*, 2012), causing the swelling of the fibres. With this method, it is possible to achieve nanofibers with small width and high fibrillation yield (Alves *et al.*, 2019).

The above-listed methods reduce the required energy for the mechanical approaches used in the preparation of NFC, which are, mainly, high-pressure homogenization, grinding, twin screwing extrusion and high-intensity ultrasonication.

High-pressure homogenization consists in the disintegration of the cellulose fibres, by passing cellulose fibres through a gap between an impact ring and a valve, in a homogenizer, under high pressure and velocity (Xie *et al.*, 2018). Used solely, this method presents a tremendous disadvantaged related to the energy consumption, that can reach up to 70 MWh/t and, when using raw materials with long cellulose fibres, the equipment often clogs. However, if combined with a pre-treatment (either one of the above mentioned), the energy requirements can be reduced to around 2 MWh/t, solving, at the same time, the clogging problems associated with this method (Eriksen *et al.*, 2008).

In the grinding method, also known as ultrafine friction grinding, the cellulosic materials are sent to a grinding area, that includes two discs – one movable and one fixed – where the NFC is obtained through high-speed grinding and shearing, with diameters from 20 to 90 nm. Some chemicals can be included in this process, to accelerate it, such as kaolin or calcium carbonate. Considering the strong mechanical force applied during the grinding, some serious damage is often inflicted to the fibres, lowering the physical strength and crystallinity of the NFC, and decreasing its thermal stability (Xie *et al.*, 2018).

Conversely, twin screwing is a very promising method for scale production, allowing the obtention of NFC fibres with diameters of approximately 30 nm. The pulp is fibrillated by two corotating and intermeshing screws (Xie *et al.*, 2018), resulting in NFC with high solid contents (25 – 40% wt) making it beneficial for transportation and storage. On the other hand, at high solid contents, NFC can form irreversible agglomerates (hornication), which compromises the re-dispersibility in solvents, required for further industrial applications (Ho *et al.*, 2015).

Besides the three listed alternatives, there is a method that requires less energy, thus having lower costs while maintaining high yields – ultrasonication. The cellulose fibres are disaggregated into smaller particles due to the strong mechanical stresses caused by cavitation, *i.e*, the formation, expansion, and explosion of microscopic gas

bubbles when liquid molecules adsorb ultrasound emissions (Wang and Chen, 2009). Through ultrasonication parameters adjustment (power and time), it is possible to manipulate the size and amount of NFC produced. In general, higher power and time of sonication results in higher yield and smaller particle sizes (Frone *et al.*, 2011).

2.2. Fibrous Clay Minerals

Fibrous clay minerals, with a special focus on sepiolite and palygorskite, will be used as fillers in the development of composite films in the present work. To properly understand the composite films' properties and behaviour upon incorporation, it is important to explore the structure, morphology and characteristics of these types of minerals.

Both sepiolite and palygorskite are encompassed in the phyllosilicate mineral category, sharing the same basic structure. These minerals are composed of six interconnected rings of SiO_4^{4-} tetrahedra, where 3 of those 4 oxygens are shared with other tetrahedra, originating a basic structural unit of $Si_2O_5^{2-}$, as represented in **Figure 3** (Nelson, 2015).

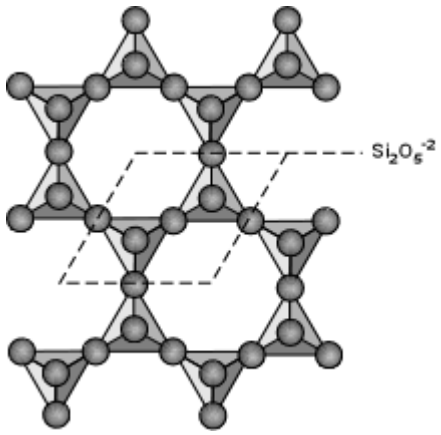

Figure 3. The basic structure of phyllosilicates (Nelson, 2015).

In the centre of the 6 membered rings, there is an OH^- ion group, which promotes the bonding of cations, such as Mg^{2+} or Al^{3+}, in octahedral coordination. If these bonded cations are 2+, all the octahedral layers sites will be occupied, taking a brucite like ($Mg(OH)_2$) structure. In the event of a 3+ bonded cation it will take a gibbsite like ($Al(OH)_3$) structure (Nelson, 2015).

Between the previous structural units, there is an empty space known as interlayer space. This can be occupied by water molecules or metal cations, which can increase the distance between two successive layers. When a significant interaction between those layers is still present, the phenomenon is called delamination, and some of the crystallographic orientation is maintained. At some point, the two layers stop interacting, becoming independently mobile in the liquid phase, and this event is known as exfoliation. Both these phenomena have a strong influence in the properties of the nanoclays, especially regarding gas barrier (Alves *et al.*, 2019).

The greatest challenge associated with the use of minerals is their dispersion in the matrix, *i. e*, obtaining intercalation and exfoliation. Some strategies have been studied to improve the dispersibility of clays, by disaggregation of the crystal bundles. These methods can be mechanical, chemical or a combination of both.

Mechanical processes are intended to destroy the larger bundles present in the nanoclays into smaller ones, while avoiding damage to the crystal structure (Alves *et al.*, 2019), and are divided into dry and wet methods. Dry methods are simpler and have a lower cost than the remaining, can be adapted for large-scale treatments and discard the need for solvents. Examples of dry processes are extrusion, ball grinding or stone milling. Nevertheless, the mechanical forces applied to the minerals may end up breaking or reducing the length of the nanorods of fibrous minerals, which are the main characteristics that provide the excellent properties to these minerals. Despite requiring much water, wet methods are preferred, being capable of achieving high disaggregation efficiency and causing lower damage to the nanorods. Examples of these processes are high-speed shearing and ultrasonication. High-speed shearing applies shearing, impact and dispersion forces, allowing to disaggregate the bulk and even enhancing the viscosity. Ultrasonication loosens the aggregates, thus favouring the dissociation of the material, however, it is not adequate for large-scale applications (W. Wang and A. Wang, 2015).

Chemical methods consist in the alteration of the surface's chemistry, to break the electrostatic, hydrogen-bonding and Van der Waals' forces among rods. The working principles of chemical methods are the alteration of the interactions through the addition of new molecules or ions, the dissolution of the internal impurities so that the bundles become more breakable, and the introduction of larger molecular chains followed by the increase of the repulsion among rods. When recurring to these processes, moderate

chemicals should be used, as they might lead to changes in the surface features (W. Wang and A. Wang, 2015).

2.2.1. Palygorskite and Sepiolite

While belonging to the phyllosilicates' group, these two minerals differ from the remaining group members by having the apical oxygen atoms pointing away from the basal oxygen atom plane, forming a ribbon-like pattern. The ribbons with apices pointing up are vertically linked to ribbons with apices pointing down, by forming octahedral coordination groups around Mg and Al. This way, a 2:1 layer is formed, being the tetrahedral sheets continuous across ribbons, but with their apices pointing in a different direction, thus a discontinuous octahedral sheet (Bailey, 1980).

Due to this characteristic, a new group is considered, known as the palygorskite-sepiolite group, which includes, aside from palygorskite and sepiolite, falcondite, kalifersite, loughlinite, raite, tuperssuatsiaite and yofortierite (Guggenheim and Krekeler, 2011). Minerals included in this group, feature continuous tetrahedral basal oxygen plans, inverted tetrahedral arrangements and discontinuous octahedral sheets (Birgatti *et al.*, 2013). In **Figure 4**, the structure of both palygorskite (attapulgite) and sepiolite is represented, retrieved from Millot, 1970.

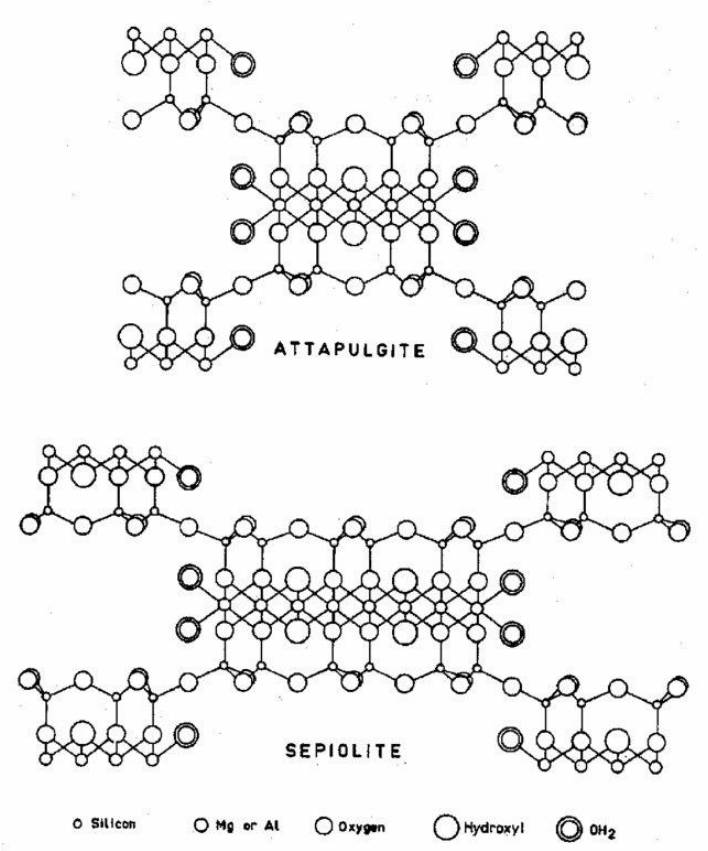

Figure 4. Structure of palygorskite (attapulgite) and sepiolite (Millot, 1970).

These materials have excellent sorptive functionality, which includes both absorption and adsorption, that depends not only on their capillary structure, surface area, negative charge and active sorptive groups but also on the characteristic of the liquid or gas to be adsorbed or absorbed (Miles, 2011). Their sorption capacity is controlled by the mineral fibre surfaces and zeolitic-like channels, which are channels containing water molecules (zeolitic water) and exchangeable cations (Na^+, K^+, Ca^{2+}, *etc*), similarly to zeolites, where exchanges of metal cations or small cation complexes occur. The mineral-fibre surface contains i) silanol groups (SiOH), ii) surficial oxygen atoms, iii) structural water, that differs from zeolitic water, as these molecules are bound to each formula unit and participate in the coordination of the octahedral Mg and Al, and iv) broken bonds. All these characteristics allow organic molecules and other cations to interact with the mineral surface. The existence of defects in the structural unit, such as open channel defects, *i. e*, the omission of single or multiple 2:1 layer ribbons in a fibre, lead to an increase of the mineral's specific surface area, with minor to negligible influence on its sorptive properties (Krekeler and Guggengheim, 2007; Bailey, 1980).

Palygorskite, also known as attapulgite (ATT), is a naturally occurring mineral with the formula $(Mg,Al)_2Si_4O_{10}(OH)•4(H_2O)$. It is considered a fuller's earth, which are natural materials that are characterized by their high adsorptive capacity, also having the capability to decolourize oil or other liquids, without using a harsh chemical treatment (Hosterman and Patterson, 1992). The fibrous nature of palygorskite and its high surface area and porosity, give rise to excellent adsorption and gelling properties. This mineral is often used in the form of granules, for adsorption purposes, in pet litter, as a clarifying or suspending agent, and as a thickener in water or organic-based systems (Govt. of South Australia, n.d.).

Ideally, a palygorskite crystal should be a trioctahedral mineral, with all octahedral sites occupied by Mg^{2+} ions. However, these ions can be replaced by trivalent ones (Fe^{3+} or Al^{3+}), which forms dioctahedral or intermediate structures, causing crystallographic defects in the octahedral sheets. The existence of defects has a very important role on palygorskite, by providing it with a higher aspect ratio (AR), better CAE and endowing it more pores and affluent surface groups. The combination of these characteristics ensures excellent colloidal, sorptive and reinforcing properties, while at the same time maintaining a remarkable thermal and mechanical stability. To fully take advantage of this mineral's properties, it is necessary to have the palygorskite's rods individualized or highly dispersed, hence the need of the aforementioned techniques (W. Wang and A. Wang, 2015).

Sepiolite has the formula $Mg_4Si_6O_{15}(OH)_2•6(H_2O)$ and it is mainly used for pet litter purposes (¾ of sepiolite's applications), though being commonly used as a filler (for the cosmetic industry), carrier (in insecticides/herbicides and catalysts) and as a thickener, among other uses. Its capability as thickener results from the fibrous shape of the particles, becoming less dependent on salt concentration and cation presence (Harvey and Lagaly, 2013). Sepiolite has a remarkably high external surface, caused by its lath shape, but it presents an even higher internal surface area, due to the existence of void channels on its internal structure (Miles, 2011). This mineral is characterized by its negative charge, with a zeta potential of around -20mV at a pH value of 7, which is justified by the substitution and slow leaching of Mg^{2+} (Liu *et al.*, 2017).

2.3. Hybrid organic-inorganic composite films

The previously described materials (NFC and nanoclays) can be combined into a composite, to attain improved mechanical and gas barrier properties, as well as higher thermal stability and lower cost. The existing solutions for gas barrier purposes have some drawbacks associated, for instance, the cost, water sensitivity and opacity, thus the necessity of finding viable alternatives like the combination of cellulose-derived materials with nanoclays. Several studies were conducted using planar minerals, such as vermiculite, smectite or montmorillonite (MTM), being fibrous-like ones less exploited, such as palygorskite and sepiolite, which increases the interest in developing new composites using this type of materials.

The quality and efficiency of the formed composites rely heavily on the matrix's and filler's morphological (aspect ratio and volume fraction) and surface properties (charge, energy, or Lewis' acid-base properties). It may prove difficult to control these properties, as it may require techniques that are not always available (Gamelas and Ferraz, 2015). There is also the need to ensure a good filler/matrix affinity since it affects the dispersion quality in an aqueous medium. A poor affinity between those will lead to flocculated composites, with aggregates being formed inside the matrix. On the other hand, great mechanical properties can be achieved with a good affinity between the matrix and the filler. This is caused by the formation of exfoliated structures of clay, destroying the clay's clusters, which allows its homogenous distribution in the matrix (Alves *et al.*, 2019; Arora and Padua, 2010).

When using NFC as matrix and vermiculite nanoplatelets as filler, it was possible to take advantage of the nanocellulose's reduced dimensions and the mineral's high AR. This produced a composite with better oxygen and water vapour barrier properties, compared to commercial packaging materials or pure nanocellulose, even at high relative humidity conditions of 80%. These properties are enhanced with the exfoliation level and orientation of the clay since longer diffusion paths are associated with a lower transmission rate of the gases (Aulin *et al.*, 2012). However, other authors reported the loss of mechanical characteristics with increased inorganic content, leading to a low strain to failure when using over 5% wt of MTM, which was associated to the formation of larger agglomerates (Liu *et al.*, 2011).

Some remarkable results were also achieved with TEMPO-oxidized NFC, whether using MTM or synthetic saponite. With MTM, a high Young's modulus (above 18 GPa) was maintained in composites with 5% to 50% wt in MTM content. However, the transparency decreased with increased mineral content. The hybrid composite formed with 5% wt MTM was the one that provided the best results in mechanical properties, shown in **Table 1** (Wu *et al.*, 2012). When saponite was used, high transparency was achieved at higher filler contents. These composite films were flexible and foldable, which is adequate for printed electronics applications, and showed improvements in their mechanical properties up to 10% wt saponite, decreasing afterwards (Wu *et al.*, 2014). **Table 1** also exhibits the mechanical properties of the 10% wt saponite film.

Table 1. Comparison between results obtained for mechanical properties by Wu *et al.*, 2012 and Wu *et al.*, 2014, using TEMPO-oxidized NFC with MTM and saponite.

	Wu *et al.*, 2012 (TEMPO NFC + 5% wt MTM)	Wu *et al.*, 2014 (TEMPO NFC + 10% wt saponite)
Tensile Strength (MPa)	509	425
Young's Modulus (GPa)	18	14.5
Enlongation at break (%)	7.6	10.2

Another study with MTM was also conducted by Tayeb and Tajvidi, ascertaining the influence of crosslinkers in the NFC matrix. In this study, two crosslinking agents were used – polyamidoamine epichlorohydrin (PE) and acrylic resin (ACR) – with the purpose of enhancing the MTM capacity of controlling the film's water vapour transmission rate, as well as increasing its internal bonding. Unlike Wu *et al.*¸ 2012, films with 5% and 10% wt MTM showed lower strength values than pure NFC films, which was caused by the clay interference in the hydrogen bond arrangement of the matrix. However, upon the incorporation of 1.5% wt of crosslinker, there was a significant improvement on the tensile strength (30 MPa higher than pure NFC), that was even further enhanced with a curing process applied to the films. PE-films gave better results

than ACR-films, and both were improved by the curing process, except regarding their strain-to-failure value, which was higher while uncured. Overall, the resulting NFC/MTM films were reported to exhibit good flexibility and foldability, achieving up to 130 MPa, 5.5 GPa and 9% tensile strength, Young's modulus, and strain-to-failure values, respectively (Tayeb and Tajvidi, 2018).

Fibrous minerals were also subject of research, as they have good properties mentioned in **Chapter 2.2**. To take full advantage of sepiolite's flame retardancy characteristics, it is possible to combine it with NFCs to create a film with improved fire resistance, thus countering one of the grand disadvantages of cellulosic films. Wicklein *et al.* produced hybrid films with 54% wt TEMPO-oxidized NFC and 35% wt sepiolite, incorporating 11% wt boric acid, which is the most commonly used flame-retardant agent for cellulosic materials (Wicklein *et al.*, 2016). Boric acid provides a glass-like coating on the surface that becomes exposed to the fire, also promoting polymer dehydration and char formation, which poses as a physical barrier, thermally insulating the surface and limiting the heat transfer (Ghanadpour *et al.*, 2018). These properties were reported to be pH-dependent, with the ability of, when under combustion environments, extinguishing the fire on the surface after a few seconds, for neutral pH of the composite preparation. When the hybrid composite was prepared at pH = 10, its surface did not ignite, which is associated with the high degree of NFC esterification. Under the study's conditions, the composite's pore and wall microstructure was kept intact after the tests, without signs of degradation (Wicklein *et al.*, 2016).

Ghanadpour *et al.* tested films produced from a phosphorylated NFC (P-NFC) matrix and using 10% wt of sepiolite (P-NFC/SEP) as filler. The pure P-NFC film inherently showed better flame-retardant properties than other NFC's types, as a result of the phosphate groups which promote the char formation. Due to the sepiolite's porous nature, there was a release of zeolitic water present in the channels, upon heating, which retarded the cellulose degradation, thus improving its heat resistance capacity. Regarding gas barrier properties, P-NFC/Sep presented poorer results than pure P-NFC films, which is associated with the hygroscopic characteristics of clays, causing swelling and creating a new site for the oxygen to pass through. Light transmittance (LT) at the visible range was also analysed, with results of over 75% transmittance at 600nm for P-NFC/SEP. This high value is explained by the low clay content used, as well as the removal of clay aggregates during the film preparation (Ghanadpour *et al.*, 2018).

The quality of the NFC-clay dispersion and mixture, as well as its properties, will influence the properties of the prepared coating film. Liu *et al.* tested medium (MNFC) and high (HNFC) charge density NFCs in a dispersion with sepiolite. With this study, it was shown that HNFC formed a self-standing hydrogel at lower concentrations (0.25%) than MNFC (0.5%). This gelation threshold depends on the charge density and concentration of fibrils, and higher values of charge density lead to higher viscosities (2.5x higher than MNFC at the same concentration), which delays the sedimentation time of sepiolite, increasing the long term stability of the composite dispersion. These HNFC with sepiolite were reported to be transparent, because of fewer existent agglomerates and a higher level of defibrillation (Liu *et al.*, 2017).

Liu *et al.* investigated the reinforcing effect of nanocellulose-attapulgite (NCA) composites in polypropylene (PP). Promising results were obtained when incorporating up to 3% wt of the NCA in the PP matrix, with an increase in its tensile strength, by 14.7% higher than pure PP. The reinforcing capacity associated with this attapulgite's composite is related to its toughening effect, caused by its granular structure, small cohesive energy and high shear sensitivity (Liu *et al.*, 2019).

Wang *et al.* also used ATT as filler for a regenerated cellulose matrix, to test the film's suitability for packaging purposes. The composite film showed good optical transparency for thicknesses of ca. 60 μm, allowing to see through the inside, which is explained by a homogeneous distribution of the ATT in the cellulose matrix. A nanocomposite with 5% wt ATT could be used for commercial packaging, although further increasing its ATT content lead to a lower transparency and colour change, as a result of the formation of agglomerates. Regarding mechanical properties, the film's tensile strength and Young's modulus were improved from 86.9 MPa and 4 GPa to 127 MPa and 5GPa, respectively, for a 5% wt ATT content. This mechanical upgrade is explained by the mineral's properties, mostly its high AR and rigidity, as well as its ability to strongly interact with the matrix. Oxygen permeability was also tested at 50% relative humidity, with OTR values decreasing from 0.449 to 0.359 $cm^3.\mu m.day^{-1}.m^{-2}.kPa^{-1}$ for a pure cellulosic film and a composite with 5% ATT, respectively. Increasing the composite's mineral content leads to a lower OTR, due to the higher tortuosity of the path (Wang *et al.*, 2018).

2.4. Film Preparation Methods

To prepare composite films, different techniques can be used, which will lead to different properties of the film. Essentially, these are obtained from diluted dispersions of the desired nanoclays and NFC, followed by the removal of its solvent.

The most used methods for their preparation from aqueous dispersions are solvent casting and vacuum filtration, being the latter usually followed by hot pressing. However, there are other less used methods, for instance, solvent exchange, pre-cooling followed by freeze casting and drying, and a layer-by-layer deposition method that forgoes a drying process (Alves *et al*., 2019).

Solvent casting is a process that consists of removing the solvent (through evaporation), forming a nanofibrillar network during this process, which leads to the formation of the film. Aulin *et al* reported very good results for OTR of 0.07 $cm^3.m^{-2}.(\mu m.d.kPa)^{-1}$, while also maintaining the film's stiffness and flexibility. This technique is more efficient than others (dip or spin-coating, for instance) as it allows the preparation of larger area coatings with an acceptable thickness (Aulin *et al*., 2012). Solvent casting possesses other captivating advantages, by allowing the obtention of films with excellent transparency and low haze, also making possible the production of composite films that are resistant to high temperatures (Siemann, U., 2005). The main disadvantage associated with this method is its associated costs, as it requires an extra investment for the solvent recovery (energetically wise) and handling. In addition to this, since this technique comprises the solvent evaporation, it tends to be a slow process. Finally, another limitation associated with solvent casting is the fact that the raw material needs to be well dispersed in water or a volatile solvent, to ensure a good quality of the dispersion, thus allowing the obtention of the film (Siemann, U., 2005).

Another widely used method is the vacuum filtration one, which consists of fast solvent removal, thus concentrating the fibres at the bottom. To prevent wrinkling and speed up the drying process, vacuum filtration is often followed by a hot-pressing process, where the filtered material is submitted to pressure in an oven. This is a fairly simple process, also being the fastest method for film preparation, and achieves improved properties of the composites. The dispersions obtained from vacuum filtration have a more homogeneous character, due to the induced delamination of the clay aggregates during the process, improving its quality. Since the quality of the film depends on the

quality of the dispersion, this method allows the preparation of composite films with great functional properties (Ho *et al*., 2012; Garusinghe *et al*., 2018). There is only one major disadvantage associated with this method, which is the loss of particles of the nanoclays during the filtration process (Zafar *et al.*, 2016).

2.5. Inverse Gas Chromatography (IGC)

Inverse gas chromatography (IGC) is a widely used technique to characterize the properties of a solid's surface, such as its surface free energy, its acid-base properties, or the enthalpy/entropy of adsorption of specific molecules on the surface of the material. Contrarily to gas chromatography (GC), where the sample (mobile phase) is injected in the chromatography column, in IGC the column is usually packed with the sample to be analysed, while a gas (probe) is injected – **Figure 5**. The time that the probe takes to go through the entire column is known as retention time (t_r) and it allows the determination of the interactions that were established between the sample's surface and the probe. This retention time is relative to a reference gas (t_0), usually methane, and it is the parameter that permits the characterization of the solid's surface. When injecting very small amounts of the gas probe, this technique is denoted IGC at infinite dilution (Jones *et al.*, 2017; Aşkın and Yazıcı, 2005). A schematic comparison between GC and IGC is represented in **Figure 5**.

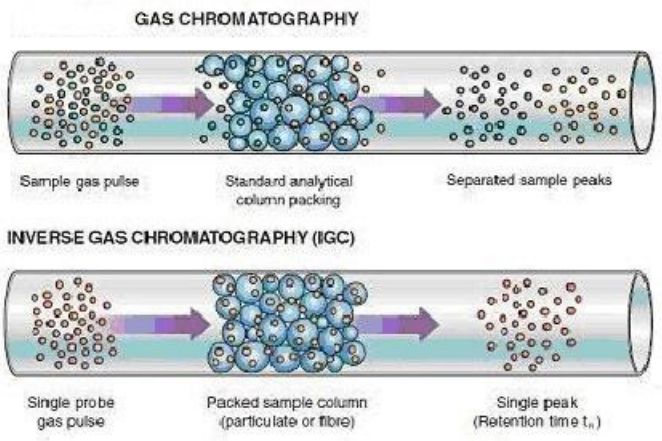

Figure 5. Schematic comparison between GC and IGC (Adapted from Milczewska and Voelkel, 2012).

To investigate a sample's surface, for instance, palygorskite, sepiolite or cellulose nanofibres, IGC is often applied with the objectives of i) estimating the dispersive

(London's) component of the surface energy, ii) obtaining some thermodynamic parameters of adsorption (standard free energy, enthalpy or entropy of adsorption) and iii) determining the characteristics of acidity or basicity of the sample's surface. The probes' type influences the property to be determined, hence the distinction between non-polar, like *n*-, branched or cyclic alkanes, or polar probes, such as acetone or dichloromethane (DCM), for example. The dispersive component of surface energy, γ^{sd}, indicates the ability of a solid's surface to have non-specific interactions with the probes, and is determined by injecting *n*-alkanes; the nanomorphology index, I_M, is obtained upon injection of branched or cyclic alkanes, and is informative about the surface's rugosity; and when injecting polar probes, it is possible to determine the specific component of the free energy of adsorption, I_{sp}, that includes all interactions between the probe and the sample, with exception to dispersive interactions, that are quantified by γ^{sd} (Boudriche *et al.*, 2011).

Upon injecting the probes, an important parameter known as net retention volume (V_N), is obtained, which corresponds to the volume of the carrier gas to elute the probe, *i.e.*, to get the probe to flow across the column. This volume is determined through **Equation 1**.

$$V_N = (t_r - t_0).F.J \quad (1)$$

where t_r and t_0 correspond to the retention times of the injected and reference probe (methane), respectively; F is the carrier gas' flow rate and J is the James-Martin corrective factor, which is given by **Equation 2** (Halasz and Heine, 1967).

$$J = \frac{3}{2}.\frac{P^2-1}{P^3-1} \quad (2)$$

where P is the absolute pressure of operation (bar).

Considering the IGC analysis is conducted at infinite dilution, it is possible to determine the free energy of adsorption of the probe (ΔG^a), per mole, through V_N, which is given by **Equation 3**.

$$\Delta G^a = -RT.\ln(V_N) + K \quad (3)$$

being K a constant that depends on the chosen reference state.

It is also possible to relate the free energy of adsorption with the work of adhesion (W^a), through **Equation 4**.

$$-\Delta G^a = N.a.W^a \quad (4)$$

with N being the Avogadro's number, *a* the probe's molecular surface area.

The work of adhesion can be related to the dispersive component of the solid (γ^{sd}) and probe (γ^{ld}) surface energy, considering the exclusive occurrence of dispersive interactions (also known as London interactions), as **Equation 5** shows.

$$W^a = 2\sqrt{\gamma^{sd}.\gamma^{ld}} \quad (5)$$

Combining **Equations 3**, **4** and **5**, the dispersive component of the surface energy can be related to the net retention volume, following **Equation 6**.

$$RTln(V_N) = \sqrt{\gamma^{ld}}.2N.a\sqrt{\gamma^{sd}} + K \quad (6)$$

Equation 6 allows the estimation of the dispersive component of surface energy for the tested solid, through a linear fit, where γ^{sd} is derived from the slope obtained from non-polar probes (Gamelas, J. A., 2013), as exemplified in **Figure 6**.

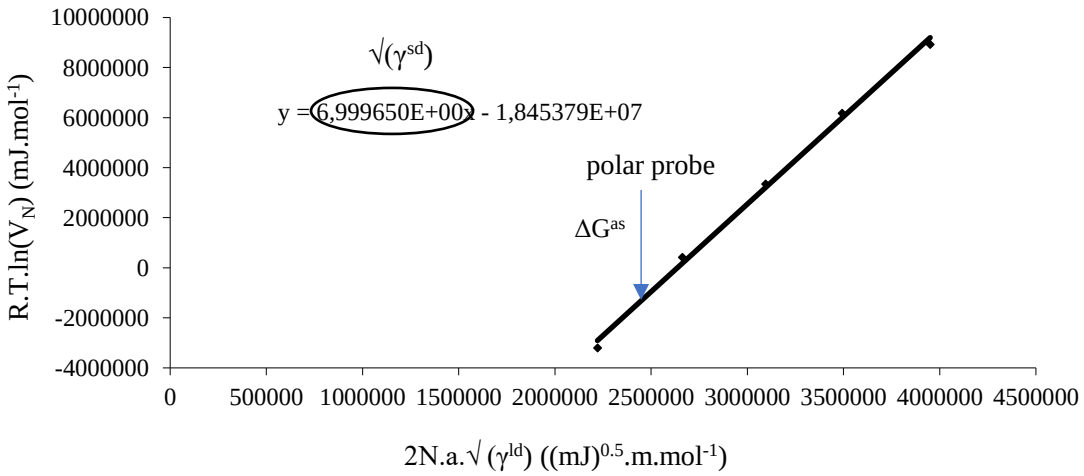

Figure 6. Example of a linear fit of RT.ln(V_N) as a function of 2N.a.$\sqrt{\gamma^{ld}}$.

The specific interaction parameters (I_{sp}) can also be determined through the linear fit represented in **Figure 6**, which allows the obtention of the specific component of the Gibbs free energy of adsorption (ΔG^{as}), and corresponds to the vertical distance between the polar probe and the *n*-alkane line.

Other relevant parameters to be determined are the specific component of enthalpy (ΔH^s) and entropy (ΔS^s), which are related to the specific component of the Gibbs free energy change of adsorption and temperature, following **Equation 7**.

$$\Delta G^{as} = \Delta H^{as} - T\Delta S^{as} \quad (7)$$

A linear fit can also be established between these variables by dividing it by the analysis' temperature, resulting in **Equation 8**.

$$\frac{\Delta G^{as}}{T} = \Delta H^{as} * \frac{1}{T} - \Delta S^{as} \quad (8)$$

Given the Gibbs free energy adsorption change and the several temperatures of the analysis, a linear representation is obtained in which the slope and intersection at origin represent the specific component of enthalpy and entropy, respectively, for each polar probe (Gamelas, J., 2013), with an example given in **Figure 7**.

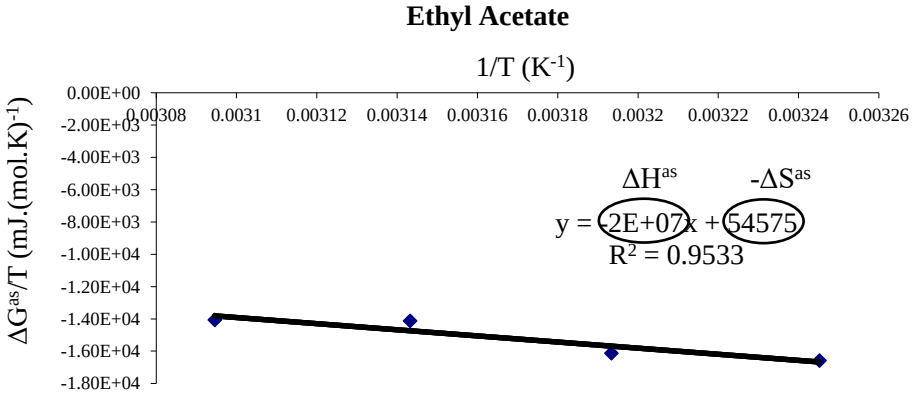

Figure 7. Example of a linear fit of $\Delta G^{as}/T$ as a function of 1/T.

Lazarević *et al.* characterized a sepiolite sample by IGC, after a 6 hours conditioning at temperatures between 210ºC and 240ºC, since the zeolitic water in sepiolite's inner channels is desorbed up to 200ºC. Higher temperatures were not used as, according to the authors, it would lead to a structural change, associated to the loss of two structural water molecules, coordinated to the Mg^{2+} ion, which also causes a decrease in the specific surface area. Upon injection of *n*-alkanes, the adsorption capacity of sepiolite was reported to increase with the higher number of carbons, translated by the standard adsorption enthalpy. Interaction strength between sepiolite and *n*-alkanes was higher than

on previous studies, which can be explained by the microporosity, the number of effective adsorption sites or specific surface area of the sepiolite sample (Lazarević *et al.*, 2009).

Other works regarding sepiolite characterization by IGC were made as the one reported by Aşkın and Yazıcı. The sample was submitted to a 24-hour conditioning at 350ºC, with probe injections carried out in a temperature range of 320ºC to 350ºC. In comparison to other planar minerals, *i. e* kaolinite or bentonite, sepiolite yielded the lowest values for γ^{sd}. The higher γ^{sd} values obtained for layered minerals is associated to the stronger retention of the *n*-alkane probes, which is caused by the irregular stacking of layers that lead to structural homogeneities. Sepiolite, as fibrous mineral, possess a higher specific area and lower crystallinity, which implies a more uniform external area, thus the smaller interaction with probes and the respective lower γ^{sd} value. It was also reported that the adsorption capacity of polar probes depends on the polarity and bulkiness of the sepiolite's surface groups (Aşkın and Yazıcı, 2005). Contrarily to Lazarević *et al.*, where the sample's surface was found to display high basicity, Aşkın and Yazıcı reported an acidic surface, indicating that the origin of the sepiolite's sample has influence on the characteristics determined by IGC (Aşkın and Yazıcı, 2005; Lazarević *et al.*, 2009).

Although experiments with sepiolite were more common than those with palygorskite, Boudriche *et al.* assessed the effect of a thermal treatment pre-applied to ATT. The ATT sample was submitted to an environment with gradually increased temperature, from 100ºC to 1000ºC, to investigate the behaviour of the sample under these circumstances, before proceeding to IGC analysis, which would allow the better selection of experimental conditions. A first mass loss, up to 160ºC was associated with the removal of water from the ATT's surface, as well as some zeolitic water present in its channels. At 280ºC, all the zeolitic water was reported to be eliminated, though at this temperature reversible phenomena could happen, because the sample was a great absorbent towards the water. At higher temperatures, the structure started to become rafter, up until the point where partial destruction of the crystalline structure happened. Similar to what has been reported in previous studies regarding IGC in clay minerals (Aşkın and Yazıcı, 2005; Lazarević *et al.*, 2009), the γ^{sd} value decreases with a temperature increase, which is caused by the disappearance of structural defects, that promote strong interactions with the probes (Boudriche *et al.*, 2011).

2.5.1. IGC relevance in film preparation

In the current project, IGC appears as an important technique, allowing the study of the compatibility between the mineral particles and the NFC. The retention time obtained through *n*-alkanes will be an indicator of a sample's dispersive component of the surface energy (γ^{sd}), which represents the potential of its surface to undergo London and Debye interactions. A higher compatibility between the NFC and the mineral is expected to be obtained at higher surface energy values. On the other hand, the retention time of polar probes gives a new set of information through the surface's acid-base properties, which is the specific component of the free energy of adsorption (I_{sp}). Once again, it is expected that the higher the I_{sp} values, the better is the composite film obtained from a certain mineral/NFC dispersion.

Furthermore, IGC is a better alternative for the analysis of rough, porous, hydrophilic, and heterogeneous surfaces, such as NFC samples, rather than the classic contact angle technique (Gamelas *et al.*, 2014). This can be done by injecting branched or cyclic alkanes, allowing the assessment of the surface's roughness, by determining the nanomorphology index (I_M). A lower I_M is associated with greater surface roughness and is linked to the γ^{sd} values (Adscientis, n.d.).

Each obtained property is an indicator of the quality of the prepared films, as it allows the prediction of the magnitude of interactions established among its components, hence the important role of IGC in the identification of the most compatible mineral/NFC compositions.

3. Materials and Methods

3.1. NFC

The NFCs used in the present work were obtained from *Eucalyptus globulus* and were subjected to different types of pre-treatments: TEMPO-oxidation, enzymatic treatment (with Enzyme 1 or Enzyme 2) and solely mechanical treatment, with their preparation process thoroughly explained below.

NFC TEMPO was prepared from bleached *Eucalyptus globulus* kraft pulp with a TEMPO mediated oxidation, followed by high-pressure homogenization at RAIZ (*Instituto de Investigação da Floresta e Papel*, Aveiro). The previously refined eucalyptus fibres (up to 4000 PFI) were dispersed in an aqueous medium, with the following reagents: TEMPO radical (0.016g per g of fibre) and NaBr (0.1g per g of fibre). The obtained mixture was stirred for 15 minutes at room temperature, to guarantee a good dispersion of all the components. Three suspensions were treated with 55 mL, 110 mL and 165 mL of NaClO – TEMPO 55, TEMPO 110 and TEMPO 165, respectively. To maintain the pH of the solution at 10, NaOH was continuously added to the mixture, with the reaction being considered completed after 2 hours, ensuring a stabilized pH of 10. Afterwards, the oxidized fibres were filtered and washed thoroughly with distilled water (to obtain a similar conductivity to distilled water), followed by mechanical homogenization (two passages) (Coelho, 2016).

The production of enzymatic NFCs also involved an initial refination of eucalyptus fibres (4000 PFI), so the fibres became more accessible. A suspension in water was prepared with these fibres, with a consistency of 3.5%, while the pH was adjusted to *ca*. 5, through the addition of sodium citrate buffer. The enzyme was added to the suspension under constant stirring, in a ratio of 300g per 1 ton of pulp (dry basis), and the process was concluded after 2h at 50ºC, followed by a 15 min heating at 80ºC, to denature the enzyme. To conclude this process, the samples were mechanically homogenized and washed with distilled water (Lourenço *et al*. 2019). The resulting NFC prepared with Enzyme 1 and Enzyme 2 were labeled as NFC-E1 and NFC-E2, respectively.

To prepare the mechanical sample (NFC Mec), a pulp previously refined up to 15000 PFI was subjected to a mechanical homogenization process (two passages).

The consistency of each prepared NFC suspension is shown in **Table 2**, in percentage (w/w, %).

Table 2. Consistency of the prepared NFC samples, in percentage (w/w, %).

Sample	Consistency (w/w, %)
NFC – Mec	0.74
NFC – E1	0.94
NFC – E2	0.80
NFC TEMPO 55	0.90
NFC TEMPO 110	0.93
NFC TEMPO 165	0.99

3.2. Fibrous minerals

Three fibrous minerals were provided: two sepiolites (SEP) obtained by different pre-treatment procedures, and palygorskite (PAL). These samples were provided by Tolsa SA (Madrid, Spain). One of the sepiolite samples has been processed by dry micronization process, using a jet mill to break the fibre bundles and reduce the particle size into micron dimensions; the other sepiolite sample was pre-treated using a wet process able to produce an extensive deagglomeration of the sepiolite fibres, without extensive breakage (Alves *et al.*, 2020).

3.3. Inverse Gas Chromatography (IGC)

The compatibility between the different minerals and the different NFCs was ascertained using an IGC analysis in a DANI GC 1000 digital pressure control gas chromatograph, equipped with a hydrogen flame ionization detector. The mineral samples were introduced in a 40cm stainless steel column while for the NFC samples were used 50cm stainless steel columns, with glass wool on both ends of the columns. Each column had an inner diameter of 4 mm and was previously washed with acetone and air-dried before packing. After packing, the columns were bent into a U-shape to be introduced in the equipment. **Annex I** contains supplementary data regarding the packed mass of mineral and NFC.

The mineral powder samples were compacted in a hydraulic press to a tablet-like form, to facilitate the packing process of the column and achieve an acceptable gas flow rate for the IGC analysis. These were conditioned overnight at 270ºC and measurements were made at one oven temperature only: 240ºC, with injector and detector temperatures at 180ºC and 200ºC, respectively. The NFC samples were initially lyophilized and grinded in a coffee grinder before being packed in the column. All NFC samples were conditioned overnight at 105ºC before the analysis, and four temperatures were measured (35ºC, 40ºC, 45ºC and 50ºC), with both the injector and detector temperatures set at 150ºC.

Helium was used as the carrier gas, and its inlet pressure was defined at 240ºC and 35ºC, for minerals and NFC, respectively, according to the retention time of octane (inlet pressure was manipulated to achieve an octane retention time of ca. 1min at 35ºC), and kept constant throughout the remaining temperatures. Air and hydrogen flow were set at a pressure of 1.05 bar and 0.8 bar, respectively.

Polar and non-polar probes were injected in all samples in small quantities of vapour (< 1μL). The non-polar probes used were pentane (C_5), hexane (C_6), heptane (C_7), octane (C_8), nonane (C_9) and decane (C_{10}). The NFC-Mec sample was evaluated with C_5 to C_9, while the remaining NFC samples were injected with C_6 to C_{10}. The polar probes used in this procedure were acetone (C_3H_6O), dichloromethane (DCM, CH_2Cl_2), trichloromethane (TCM, $CHCl_3$), ethyl ether ($(C_2H_5)_2O$), tetrahydrofuran (THF, C_4H_8O) and ethyl acetate (ETA, $C_4H_8O_2$). Methane (C_1) was injected in every sample as the reference probe.

Since some of the chromatograms behave as an exponential function, two to three peaks of each probe between 3V and 10V were needed to be obtained, to minimize its variation with intensity (linear section of the exponential curve). The retention time of each probe was the average of these measurements. **Figure 8** shows an example of a chromatogram.

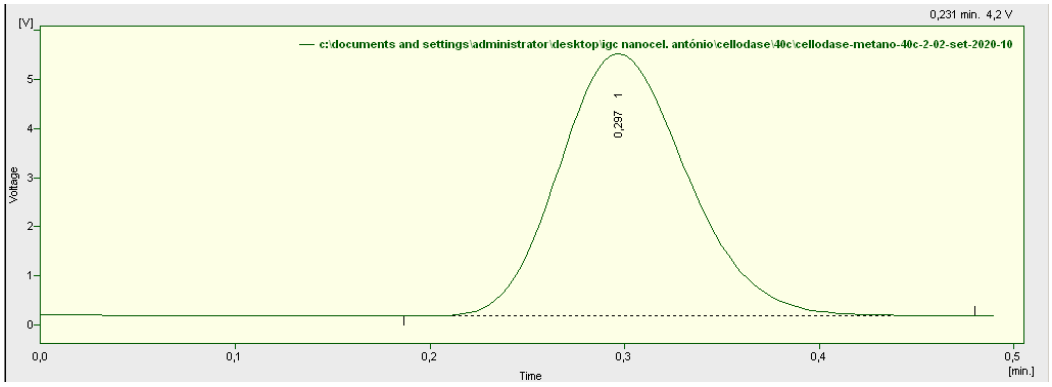

Figure 8. Example of a chromatogram, for methane in an NFC-E2 sample.

3.4. X-Ray diffraction analysis

An X-ray diffraction analysis was conducted to ascertain the crystallinity of the samples, and it was performed on a Siemens D5000 X-ray diffractometer which consists of a θ/2θ diffraction instrument that operates in the reflection geometry, able to identify crystalline phases down to 3% of the bulk. The determination of the crystallinity followed **Equation 9** (Segal *et al.*, 1959).

$$Crystallinity\ (\%) = \frac{I_{002} - I_{am}}{I_{002}} * 100 \qquad (9)$$

where I_{002} corresponds to the maximum intensity of the (002) lattice diffraction and I_{am} is the intensity of diffraction at 2θ = 18º.

3.5. NFC and Composite Films

Two types of films were prepared in the present work: NFC-only films and hybrid composite films with both NFC and clays, using two different techniques – solvent casting and vacuum filtration.

3.5.1. Solvent Casting

For this method, suspensions were prepared in glass beakers, using 12.4g of NFC suspensions: NFC – Mec, NFC TEMPO 55, NFC TEMPO 110, NFC TEMPO 165 and NFC E1, and water was added to make up a total of 60g. These suspensions went through a homogenization process at 500rpm for 20 minutes, before being poured into the Petri dish.

Except for NFC TEMPO 165, two films of each sample were prepared with the solvent casting method at room temperature. A third film of NFC-E1 and NFC TEMPO 110 was also obtained with solvent casting method but with the use of an oven, at 50ºC, to accelerate the solvent evaporation process (NFC-E1(o) and NFC TEMPO 110(o), respectively). Finally, a fourth film of NFC TEMPO 110 was also prepared through solvent casting method at room temperature, although this one was preceded by an ultrasonication process for 10 minutes (NFC TEMPO 110u). However, only the films left drying at room temperature were considered in this work, for solvent casting.

Hybrid composites were prepared with 10% and 50% (dry weight) of minerals (PAL and SEP). To do so, two mineral suspensions with a 1% mineral consistency were prepared followed by ultrasonication for 10 minutes, to stabilize the suspension, to be further added to the NFC. **Table 3a** and **Table 3b** show the quantities of the suspensions that were added to achieve films with 10% and 50% (dry weight), respectively.

Table 3a. Quantities of NFC and mineral suspensions needed to prepare films with 10% mineral (dry weight).

	m NFC (g)	m mineral (g)
NFC Mec 10%	11.46	0.94
NFC-E1 10%	11.23	1.17
NFC TEMPO 55 10%	11.27	1.13
NFC TEMPO 110 10%	11.24	1.16
NFC TEMPO 165 10%	11.17	1.23

Table 3b. Quantities of NFC and mineral suspensions needed to prepare films with 50% mineral (dry weight).

	m NFC (g)	m mineral (g)
NFC Mec 50%	7.12	5.27
NFC-E1 50%	6.39	6.01
NFC TEMPO 55 50%	6.53	5.87
NFC TEMPO 110 50%	6.42	5.98
NFC TEMPO 165 50%	6.23	6.17

After NFC and mineral suspensions were weighed, distilled water was added to make up 60g, and the resulting suspensions went through a homogenization process at 500 rpm for 20 minutes, being then poured into Petri dishes so the solvent could evaporate at room temperature. For the exact quantities that were weighed into the suspension, please see supplementary data on **Annex II**.

3.5.2. Vacuum Filtration

Similarly to the procedure described in the previous section, suspensions of NFC were prepared, with the same quantities as in **Chapter 3.5.1.** (**Table 3a** and **Table 3b**). However, instead of being immediately poured into Petri dishes, these suspensions were put into a filtration system composed of two Kitasato flasks, a vacuum pump, and a filter plaque with a porosity of 45µm, with quantitative filter paper in it, being this setup shown in **Figure 9**. After concluding the filtration process, the filter paper was removed from the filter plaque and left drying over a Petri dish. Two suspensions of each NFC were prepared (either NFC only, 10% and 50% mineral), being one of them (labeled as #1) dried at room temperature, while the other one (labeled as #2), dried in an oven, at 50ºC, to accelerate the process. Finally, after the films were completely dry, they were separated from the filter paper.

Figure 9. Filtration setup, consisting of two Kitasato flasks, a vacuum pump and a filter plaque with a porosity of 45µm.

3.6. Films testing

The produced films were subjected to an elongation at break test at the Faculty of Pharmacy of University of Coimbra, using a TA.XT.Plus Texture Analyser. This test followed a standard norm known as D 882 – 02: Standard Test Method for Tensile Properties of Thin Plastic Sheeting (ASTM International [ASTM], 2018). The films were cropped into 4x4 cm shapes and attached to two grips, with a separation distance of 1 cm, that would then move in opposite directions, until rupture, as schematically represented in **Figure 10**.

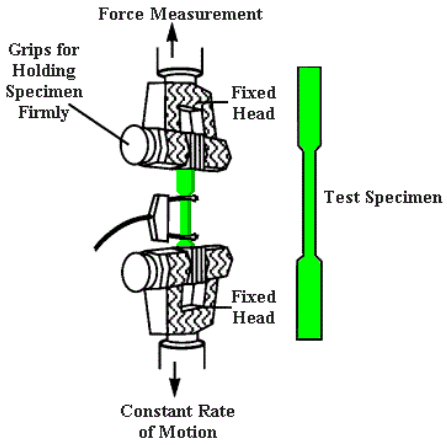

Figure 10. Schematic representation of elongation at break test.

The thickness of these films was also measured with an optical microscope, using a Olympus BH-2 195 KPA microscope (Olympus Optical Co., Ltd) equipped with a high-resolution CCD colour camera (Olympus ColorView III). Images were captured and analysed using the analySIS software (Soft Imaging System GmbH). In this analysis, small sections of the films were cropped and held vertically to the microscope's objective. The image corresponding to the border was then snapshotted and a built-in measurement tool was used to estimate the thickness of the film.

With the results from the elongation at break test, it is also possible to determine the tensile strength and elongation at break, through **Equations 10** and **11** (ASTM, 2018).

$$Tensile\ Strength\ (MPa) = \frac{F}{A} * 10^{-6} \quad (10)$$

$$Elongation\ at\ break\ (\%) = \frac{\Delta L}{L_0} * 100 \quad (11)$$

Knowing the force that was applied from the traction tests and the thickness of the films, it is possible to determine the Young's modulus (E) of the films, which corresponds to the stiffness of a material, and it is defined by the relationship between tensile stress and axial strain, in the linear elastic region of a material, as shown in **Equation 12** (Jastrzebski, D, 1959).

$$E = \frac{F/A}{\Delta L/L_0} = \frac{Tensile\ Strength}{Elongation\ at\ break} \quad (12)$$

with E being the Young's modulus, F the applied force, A the area of the cross-section, ΔL the change in the films' length and L_0 the initial length of the film.

Finally, the light transmittance was also measured, using a Jasco V-530 UV/Vis Spectrophotometer, with two quartz cuvettes, with one being the reference and the other one containing the sample. The spectral sweeping wavelength was from 800nm to 200nm, to comprise both the visible and the UV region.

4. Results and Discussion

4.1. Inverse Gas Chromatography (IGC)

IGC was used to ascertain the surface properties of the NFCs and clays samples, by injecting both non-polar and polar probes. The operating conditions used in the IGC analysis are shown in **Table 4**.

Table 4. Operating conditions of IGC analysis.

Temperature (ºC)	Operating conditions	Samples				
		NFC Mec	NFC TEMPO 55	NFC TEMPO 165	NFC-E1	NFC-E2
35	Pressure (bar)	0.9	0.1	0.05	0.07	0.05
	Starting Flow Rate (mL.min-1)	8.6	6.9	9.9	7.9	15.2
	Ending Flow Rate (mL.min-1)	10.3	6.9	9.3	7.8	15.1
40	Pressure (bar)	0.9	0.08	0.05	0.07	0.05
	Starting Flow Rate (mL.min-1)	25.9	7.5	9.8	7.8	15.4
	Ending Flow Rate (mL.min-1)	30.6	6.4	9.6	7.5	14.2
45	Pressure (bar)	0.33	0.08	0.05	0.07	0.05
	Starting Flow Rate (mL.min-1)	8.7	6.3	9.2	7.5	14.2
	Ending Flow Rate (mL.min-1)	8.8	6.2	9.2	7.5	13.7
50	Pressure (bar)	0.33	0.08	0.05	0.07	0.05
	Starting Flow Rate (mL.min-1)	9.1	6.8	8.5	7.4	13.4
	Ending Flow Rate (mL.min-1)	9.2	6.7	8.5	7.4	13.2

As exhibited in **Table 4**, the IGC analysis was conducted under constant pressure for each sample. The NFC Mec is an exception to the previous statement, as a significant change in the flow rate was verified with temperature increase from 35 to 40ºC, hence the

need to adjust the pressure to maintain a stable flow rate at higher temperatures, similar to that at 35ºC.

Before starting the analysis, both methane and *n*-octane were injected, to optimize the operating conditions, as the pressure and flow rate applied were based on these probes' retention times. As stated before, a retention time of octane between 0.7 and 1.5 minutes is desired, to allow a proper distinction between the remaining probes' retention times, while methane was once again injected as a reference probe.

For each sample and temperature, both the initial and final flow rate were measured, to ensure its deviation was minimal and thus to consider the analysis valid.

After two to three repeated injections of each probe (peak height between 3V and 10V), the mean retention time was considered. The values of the retention time at 35ºC are presented in **Table 5**.

Table 5. Retention times for all probes and NFC sample, at 35ºC, in minutes (min).

		Samples				
	Probes	NFC Mec	NFC TEMPO 55	NFC TEMPO 165	NFC-E1	NFC-E2
Non-polar	Methane (C1)	0.786	0.617	0.523	0.597	0.3
	n-Pentane (C5)	0.836	-	-	-	-
	n-Hexane (C6)	0.991	0.693	0.559	0.679	0.344
	n-Heptane (C7)	1.42	0.807	0.619	0.856	0.429
	n-Octane (C8)	2.733	1.157	0.835	1.378	0.705
	n-Nonane (C9)	6.487	2.127	1.44	2.95	1.449
	n-Decane (C10)	-	4.9	3.165	7.83	3.699
	Cyclohexane	1.069	0.703	0.555	0.678	0.364
Polar	Dichloromethane (DCM)	1.101	0.667	0.539	0.639	0.333
	Trichloromethane (TCM)	1.206	0.737	0.579	0.746	0.382
	Acetone	4.037	0.766	0.627	0.931	0.443
	Tetrahydrofuran (THF)	2.117	0.887	0.702	1.117	0.596
	Ethyl Acetate (ETA)	1.126	0.677	0.563	0.756	0.352

Ethyl Ether	2.34	0.912	0.727	1.182	0.561

From the retention times obtained with non-polar probes, the dispersive component of the surface energy (γ^{sd}) was determined. The alkanes with a lower number of carbons (*n*-pentane and *n*-hexane) had generally very similar retention times to methane, thus pentane was only injected on NFC Mec, as the probes were taking more time to leave the column, allowing the distinction of their retention times. On the remaining samples, pentane was not injected, since its retention time was very close to methane and hexane. The more the number of carbons in the non-polar probes, the higher is the time it takes for the probe to leave the column, since their molecular weight also increases.

4.1.1 Dispersive component of the surface energy (γ^{sd})

As mentioned in **Chapter 2.5.**, the dispersive component of the surface energy can be obtained through the linear fit described by **Equation 6**. These values were determined through the injection of non-polar probes (alkanes), considering that dispersive interactions occur, and are expressed in $mJ.m^{-2}$ (**Table 6**).

Table 6. Dispersive component of the surface energy (γ^{sd}) obtained for the different NFC samples.

Temperature (ºC)	Dispersive component of the surface energy ($mJ.m^{-2}$)				
	NFC Mec	NFC TEMPO 55	NFC TEMPO 165	E1	E2
35	49.0	35.3	40.3	42.7	40.4
40	45.0	34.7	39.7	37.5	35.2
45	39.8	34.3	40.5	36.2	37.1
50	44.3	36.7	31.7	36.9	39.2

It was expected to verify a decrease of γ^{sd} with the increase of the temperature, however, that was not always the case, as shown by the highlighted values in **Table 6**. The expected decrease is associated with the fact that, at lower temperatures, the gas (probe) particles have a slower movement, caused by the lesser kinetic energy, making

them more likely to interact (*Lumen*, n.d.). Since the analysis has been done at low temperatures (in the range from 35ºC to 50ºC), and there are no chemical reactions associated, a possible explanation for these events is that the samples could have suffered a structural change.

A visual comparison between all the samples is obtained by plotting them at one temperature, which is represented in **Figure 11**, for the temperature of 35ºC.

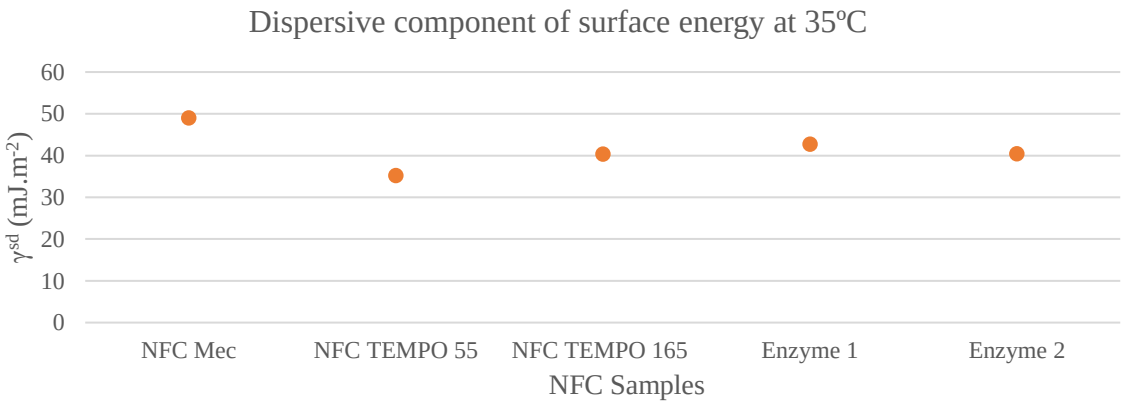

Figure 11. Dispersive component of surface energy for all NFC samples at 35ºC.

Observing **Figure 11**, NFC Mec exhibits an unexpectedly high value for γ^{sd}, which is associated with a high crystallinity of this sample. TEMPO-oxidized NFCs show slightly different values for γ^{sd} that go accordingly to theory, as higher fibrillation is related to a higher value of the dispersive component of surface energy, which is a result of having more hydroxyl groups exposed at the surface, that are said to have a greater contribution to γ^{sd} (Gamelas *et al.*, 2014). In fact, NFC TEMPO 165 is expected to present higher fibrillation than TEMPO 55, due to the addition of 165mL of NaClO, instead of the 55mL that were added to the latter mentioned sample, that promotes the formation of more carboxyl groups, which increases the fibrillation of the cellulose. The enzymatic pre-treatment tends to increase the crystallinity of the NFC, thus increasing the surface energy. However, similar values of γ^{sd} were obtained between NFC TEMPO 165 and NFC E2

To justify the aforementioned claims, a X-ray diffraction analysis was conducted to determine the crystallinity of the samples, and these results are presented in **Table 7**.

Table 7. Crystallinity of the NFC samples determined through X-ray diffraction.

NFC Sample	Crystallinity (%)
Mec	73.0
Enzymatic	68.5
TEMPO 55	67.8
TEMPO 165	69.8

NFC Mec exhibits a slightly higher crystallinity, which explains the high values for the dispersive component of the surface energy. The remaining samples show similar percentages for their crystallinity, hence the close values obtained for γ^{sd} for the enzymatic and TEMPO-oxidized samples.

At higher temperatures, the dispersive component of the surface energy tends to decrease (**Table 6**). However, at the highest tested temperature (50ºC), all but one sample (NFC TEMPO 165) showed an increase of its value, which is graphically represented in **Figure 12**.

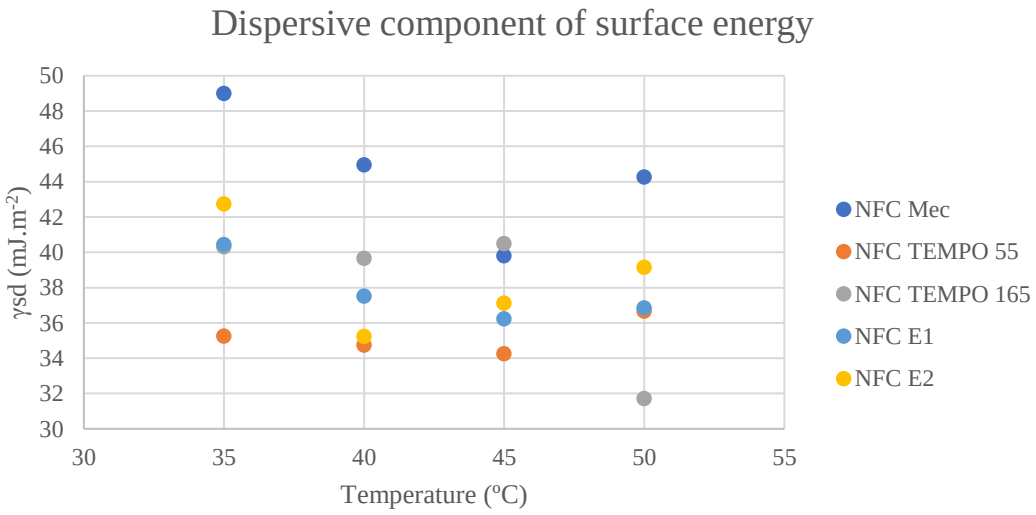

Figure 12. Dispersive component of surface energy ($mJ.m^{-2}$) as a function of temperature (ºC), for all samples.

4.1.2. Lewis acid-base character

The Lewis acid-base character of the samples is determined through the specific work of adhesion of several polar probes, able to establish Lewis acid-base interaction with the material's surface. It should be noted that the injections of polar probes for NFC Mec were discarded at 40ºC, due to a change in the flowrate through the column. **Figure 13** shows the specific work of adhesion of each polar probe obtained at different temperatures, for each sample.

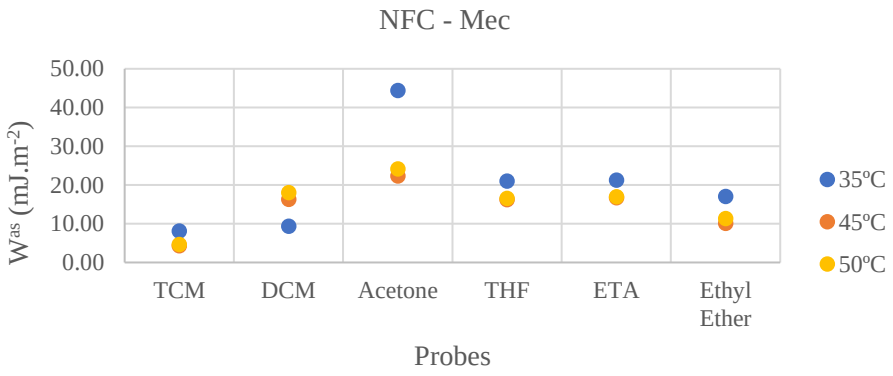

Figure 13a. Specific works of adhesion for NFC Mec, in $mJ.m^{-2}$.

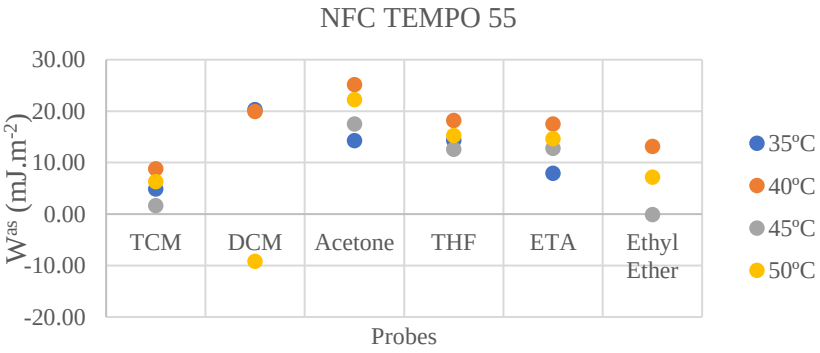

Figure 13b. Specific works of adhesion for NFC TEMPO 55, in $mJ.m^{-2}$.

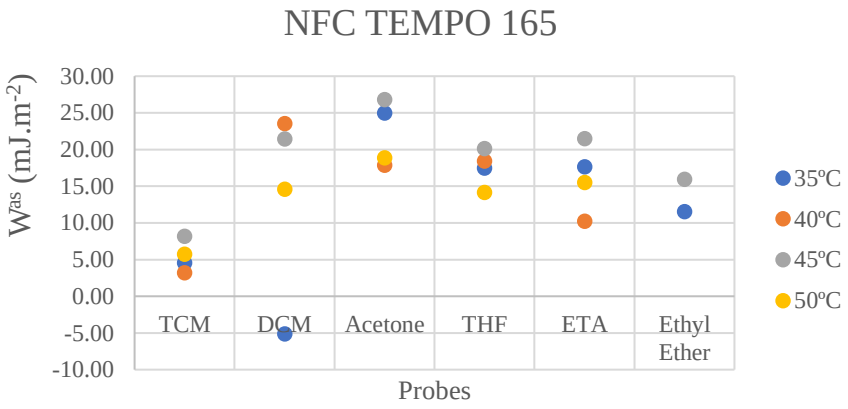

Figure 13c. Specific works of adhesion for NFC TEMPO 165, in $mJ.m^{-2}$.

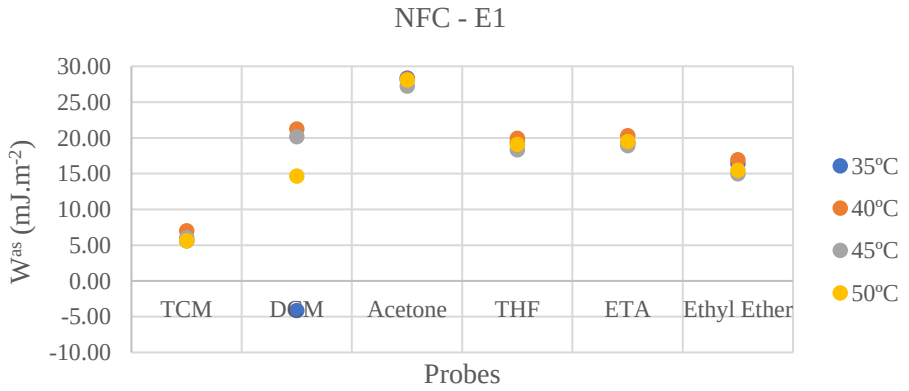

Figure 13d. Specific works of adhesion, for NFC – E1, in $mJ.m^{-2}$.

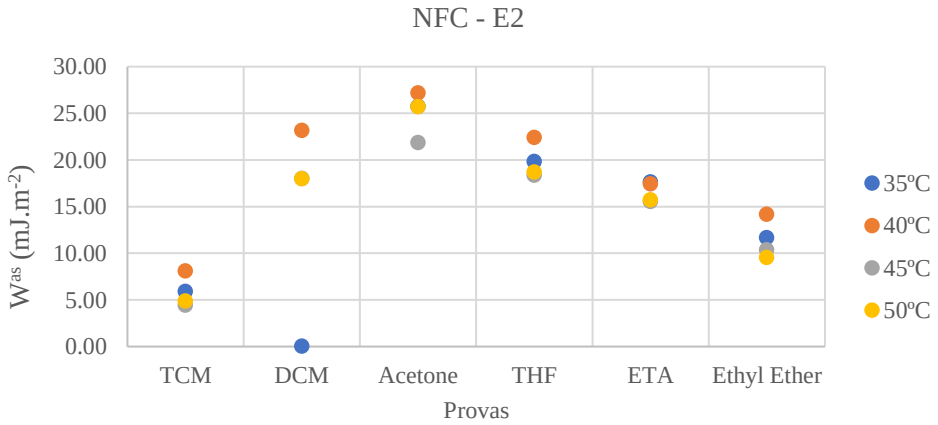

Figure 13e. Specific works of adhesion, for NFC – E2, in $mJ.m^{-2}$.

As shown in **Figure 13**, all NFC samples exhibit the highest W^{as} values for acetone, which represents a great NFC affinity with amphoteric probes. To verify the acidic or basic character of the samples, a relationship was established between the

specific work of adhesion of basic (THF) and acidic (TCM) probes, as represented by their ratio in **Table 8**.

Table 8. Ratio between the specific work of adhesion of THF and TCM, at different temperatures.

	$W^{as}(THF)/W^{as}(TCM)$			
	Temperature (ºC)			
Samples	35ºC	40ºC	45ºC	50ºC
NFC Mec	2.6	-	3.8	3.6
NFC TEMPO 55	2.9	2.1	7.8	2.4
NFC TEMPO 165	3.9	5.6	2.5	2.5
NFC-E1	3.5	2.8	3.1	3.4
NFC-E2	3.3	2.8	4.1	3.8

The ratio between THF's and TCM's works of adhesion is an indicator of the affinity of the several NFCs towards an acidic or basic probe. This ratio is always greater than 1, which implies a higher affinity of the NFC to the basic probe (THF), therefore the tested NFCs exhibit an acidic character. This affirmation is sustained by the presence of hydroxyl groups in the cellulose structure, which are associated with the acidic character of the nanocellulose surface. To corroborate the aforementioned claim, the ratio between the specific works of adhesion of ethyl ether and TCM is also exhibited in **Table 9**.

Table 9. Ratio between the specific work of adhesion of ethyl ether and TCM, at different temperatures.

	$W^{as}(ethyl\ ether)/W^{as}(TCM)$			
	Temperature (ºC)			
Samples	35ºC	40ºC	45ºC	50ºC
NFC Mec	2.1	-	2.3	2.4
NFC TEMPO 55	1.6	1.5	-	1.1
NFC TEMPO 165	2.5	3.2	2.0	-
NFC-E1	2.0	1.7	2.3	2.0
NFC-E2	2.9	2.4	2.5	2-7

Table 9 proves again a lower affinity to acidic probes (TCM), as the ratio of the works of adhesion of ethyl ether and TCM is always higher than 1. This is once more associated with the prevalent acidic character of the NFCs surfaces, also exhibiting a very good affinity for amphoteric probes (ETA and acetone), which goes accordingly to the results of **Figure 13** and previous studies (Gamelas *et al.*, 2014).

4.1.3. Specific component of enthalpy (ΔH^{as}) and entropy (ΔS^{as}) of adsorption

Besides giving an indication of the Lewis acidic or basic character of each sample, injecting polar probes also allows the determination of both the specific component of enthalpy (ΔH^{as}) and entropy (ΔS^{as}) of adsorption, through a linear relationship between Gibbs free energy change of adsorption (ΔG^{as}) and the inverse of temperature (1/T). According to **Equation 8**, ΔH^{as} and ΔS^{as} correspond to the slope and intersection, respectively, making it necessary to have a good correlation coefficient.

Regarding the NFC TEMPO 165 sample, an acceptable coefficient was only obtained when discarding the results at 45ºC, as, at this temperature, ΔG^{as} values were off the regression, being outliers. The relationship between ΔG^{as} and 1/T is represented in **Table 10**, with and without the values at 45ºC, for the different polar probes.

Table 10. Specific component of enthalpy and entropy of adsorption of the different probes, obtained for TEMPO 165, with and without values at 45ºC.

	with values at 45ºC			without values at 45ºC		
Probe	ΔH^{as} (kJ.mol^{-1})	$-\Delta S^{as}$ (kJ.mol^{-1}K^{-1}) x10^{-2}	r^2	ΔH^{as} (kJ.mol^{-1})	$-\Delta S^{as}$ (kJ.mol^{-1}K^{-1}) x10^{-2}	r^2
TCM	13.1	-4.6	0.239	7.3	-2.7	0.308
DCM	101.6	-32.6	0.724	84.3	-26.9	0.998
Acetone	-29.8	7.5	0.427	-39.3	10.7	0.992
THF	-17.2	4.0	0.251	-25.0	6.5	0.870
ETA	-10.6	1.7	0.088	-19.6	4.6	0.781

Ethyl Ether	-55.4	16.7	0.328	-76.8	23.8	0.946

When considering the values at all temperatures tested there is a poor regression. If discarding the values for 45ºC it is possible to obtain an acceptable correlation coefficient for every probe, except for TCM. Thus, the specific enthalpy and entropy of adsorption values shown in **Table 10**, can be considered valid. DCM unexpectedly presents a positive value for the enthalpy and a positive one for the entropy.

As aforementioned in **Chapter 4.1.2.**, only three temperatures were used in the IGC analysis with polar probes for the NFC Mec sample. An acceptable correlation coefficient was obtained for DCM, THF and ETA, having its visual representation in **Figure 14**, whereas the ΔH^{as} and ΔS^{as} values obtained from the remaining polar probes were discarded due to a poor fit.

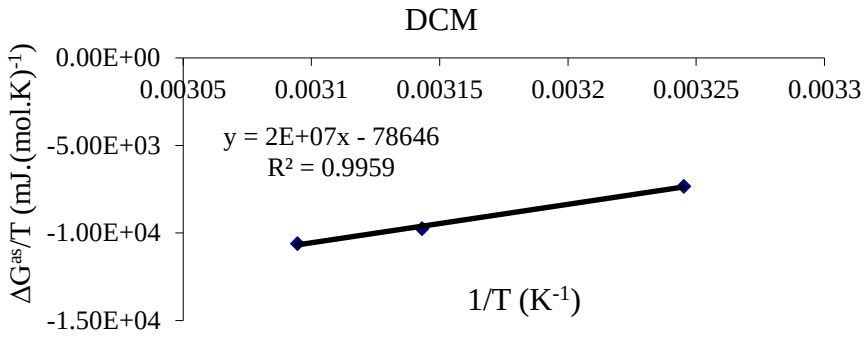

Figure 14a. ΔG^{as} as a function of 1/T for DCM for NFC Mec.

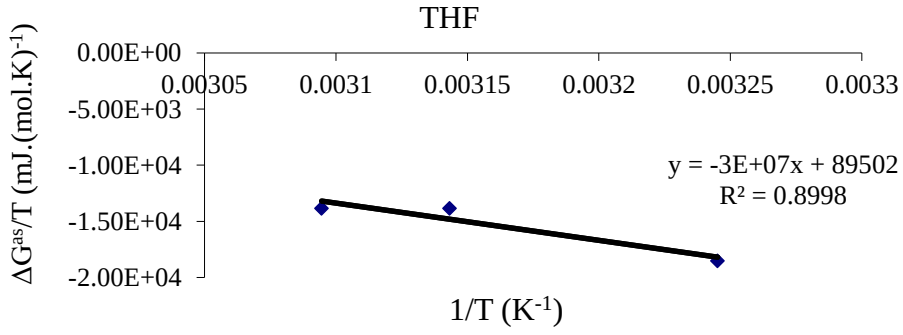

Figure 14b. ΔG^{as} as a function of 1/T for THF for NFC Mec.

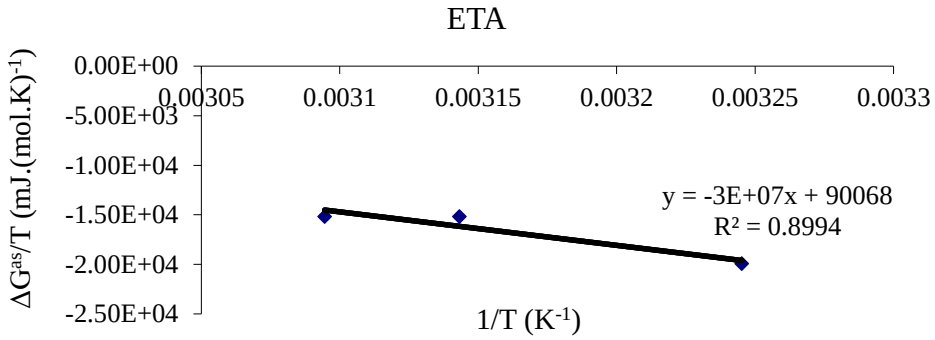

Figure 14c. ΔG^{as} as a function of 1/T for ETA for NFC Mec.

With the acceptable correlation coefficient from the linear fits shown in **Figure 14**, the specific component of enthalpy and entropy of adsorption for these probes is presented in **Table 11**.

Table 11. Specific component of enthalpy and entropy of adsorption of DCM, THF and ETA, for NFC Mec.

Probe	ΔH^s (kJ.mol^{-1})	$-\Delta S^s$ (kJ.mol^{-1}.K^{-1}) x10^{-2}
DCM	21.9	-7.8
THF	-33.2	8.9
ETA	-33.8	9.0

A positive enthalpy was once again obtained for DCM, though the system was expected to exhibit a negative enthalpy. DCM has a smaller molecular area in comparison to the other polar probes, which could be causing these unforeseen results (Shi, B., 2019).

No other samples or probes were considered, as their poor correlation coefficients led to discarding those results.

4.1.4. Sepiolite and Palygorskite IGC Analysis

Sepiolite (SEP) and Palygorskite (PAL) samples also had their surfaces analysed by IGC, to predict the compatibility with the tested NFCs. **Table 12** shows the results obtained for the dispersive component of the surface energy (γ^{sd}).

Table 12. Dispersive component of surface energy (γ^{sd}) for sepiolite (SEP) and palygorskite (PAL) samples, at 240ºC.

Mineral Sample	γ^{sd} (mJ.m^{-2})
SEP	115.9
PAL	83.4

A higher value for the dispersive component of the surface energy was obtained for the sepiolite sample. Considering that the higher the γ^{sd} value, the higher the tendency of the system to undergo London and Debye interactions, it is expected to obtain better films with sepiolite rather than with palygorskite. Other studies showed varied values for the dispersive component of the surface energy of sepiolite, ranging from 84 mJ.m^{-2} (Aşkın and Yazıcı, 2005) to 130 mJ.m^{-2} (Lazarević *et al.*, 2009) at 320ºC and 240ºC, respectively, being the latter value more in compliance with those obtained in the current work. On the other hand, the γ^{sd} value obtained for the palygorskite sample considered on the present work was well below those reported in literature, of 164 mJ.m^{-2} (Boudriche *et al*., 2010).

When injecting the typical polar probes in these mineral samples, either no signal or very insignificant signals were obtained, thus sepiolite's and palygorskite's Lewis acid-base character was not assessed, as well as the specific component of the enthalpy and entropy of adsorption of polar probes.

4.2. NFC-based films

Several different films were produced using either a solvent casting or a vacuum filtration approach. Each technique was applied to pure NFC and to suspensions with 10% and 50% (w/w) of mineral. In **Figure 15** the films obtained through solvent casting are shown, for each NFC sample, to allow visual comparison between them.

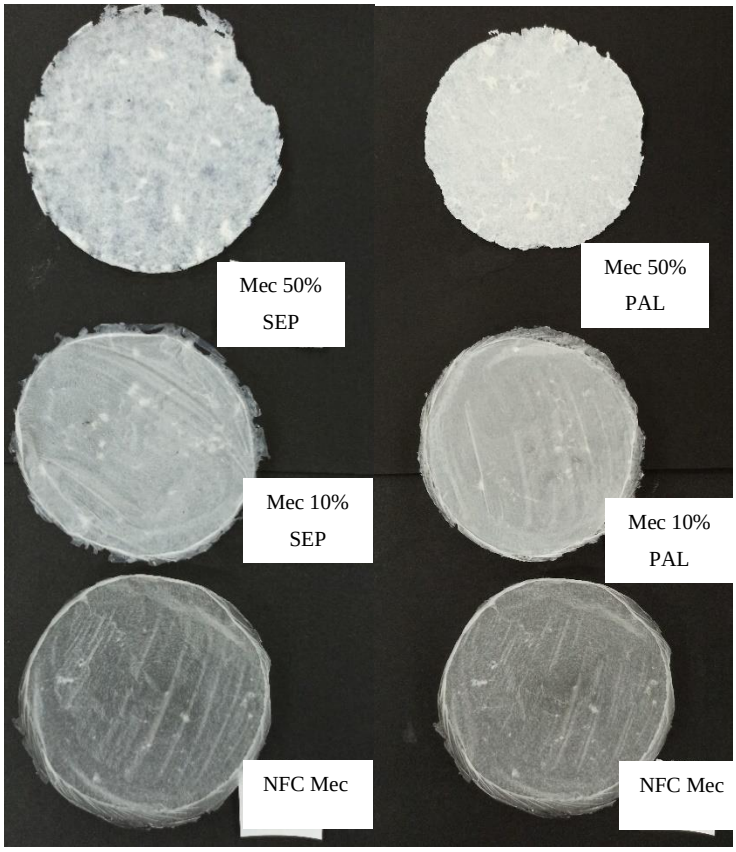

Figure 15a. Composite films for NFC Mec with 0% mineral (bottom), 10% mineral (middle) and 50% mineral (top), produced through solvent casting.

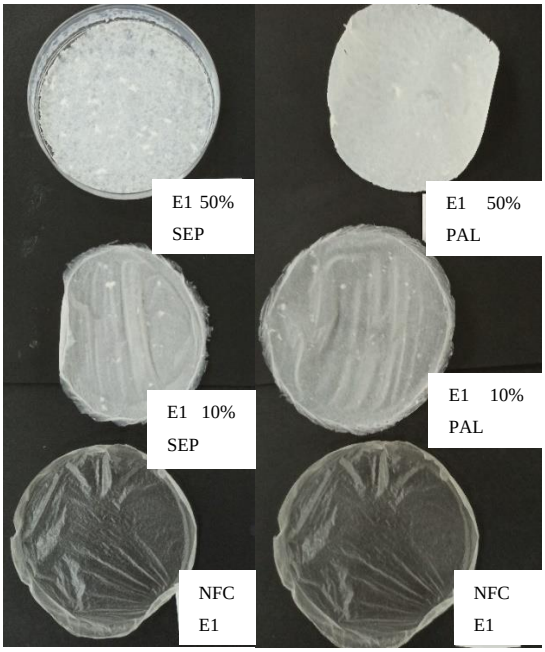

Figure 15b. Composite films for NFC-E1 with 0% mineral (bottom), 10% mineral (middle) and 50% mineral (top), produced through solvent casting.

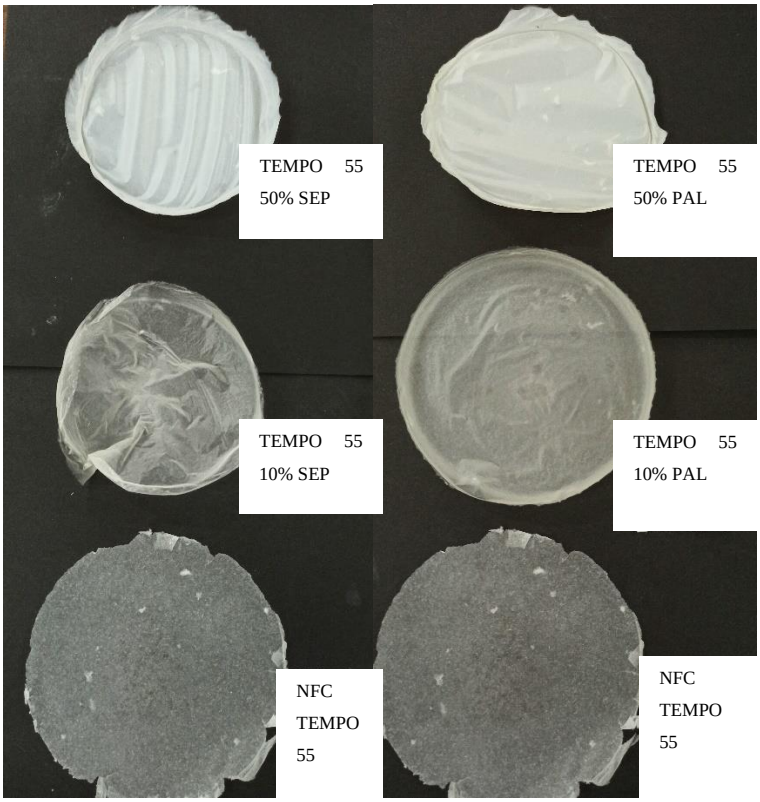

Figure 15c. Composite films for NFC TEMPO 55 with 0% mineral (bottom), 10% mineral (middle) and 50% mineral (top), produced through solvent casting.

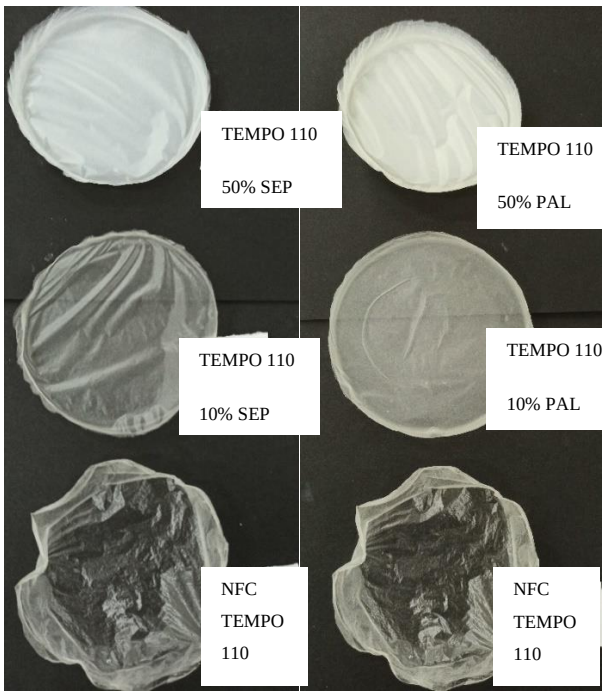

Figure 15d. Composite films for NFC TEMPO 110 with 0% mineral (bottom), 10% mineral (middle) and 50% mineral (top), produced through solvent casting.

Figure 15e. Composite films for NFC TEMPO 165 with 0% mineral (bottom), 10% mineral (middle) and 50% mineral (top), produced through solvent casting.

The films shown in **Figure 15** were all prepared using the solvent casting technique. Since this is a slow process (can take weeks, depending on the room temperature and humidity), films with good visual aspect were obtained, with relatively low curling and wrinkling.

Comparing samples, films of NFC Mec (**Figure 15a**) are very opaque, even without incorporating minerals, which is justified by the low fibrillation degree that a mechanical-only treatment induces. In addition to the low transparency, certain fibre spots are also visible, being these films of very low quality regarding optical properties. NFC-E1 films (**Figure 15b**) are somehow similar to those obtained from NFC Mec, albeit being more transparent when no minerals are incorporated.

The best results in terms of optical properties were achieved with the TEMPO-oxidized NFC, as these films (**Figures 15c**, **15d** and **15e**) exhibit a higher transparency than those from NFC Mec and NFC-E1. Observing the films from NFC TEMPO 55 (**Figure 15c**), it is already possible to see through the ones with 10% mineral, which was not possible in the previous samples obtained from NFC Mec and NFC-E1. It was

possible to observe that, as the added quantity of NaClO used in NFC pre-treatment was increased, the better the visual aspect of the obtained films. With NFC TEMPO 110 and NFC TEMPO 165, the background is clearly visible even for films with 10% mineral. There is, however, a notable difference between the opacity (visually assessed) of the films prepared with 10% SEP and those with 10% PAL, as the ones using SEP are more transparent than the PAL ones. This is valid for all the NFC TEMPO samples, where it is observable that PAL films present a yellow tone, in comparison to SEP ones. Even though the films with 50% mineral are still very opaque for all NFC samples, those with SEP still show a whiter tone and are slightly more transparent than PAL films. This suggests a better compatibility of the NFCs with SEP rather than with PAL, which was expected after a higher dispersive component of the surface energy was achieved in IGC analysis. The visible wrinkling in some of these films is associated with the solvent evaporation from the Petri dish, which made the films adhere to the plaque's wall, hence the wrinkled aspect. An explanation for this wrinkling could be the use of a stiff surface (Petri dish) to hold an elastic substrate (NFC), which will cause the phenomenon upon evaporation of the solvent, that leads to a mismatch of the strain of these two layers (Lu, X., 2019).

Previously, in **Figure 15**, a comparison was established between samples prepared with the same NFC type, though it is possible to compare between different NFC samples. To do so, in **Figure 16**, films with the same quantities of different NFC are presented, side by side.

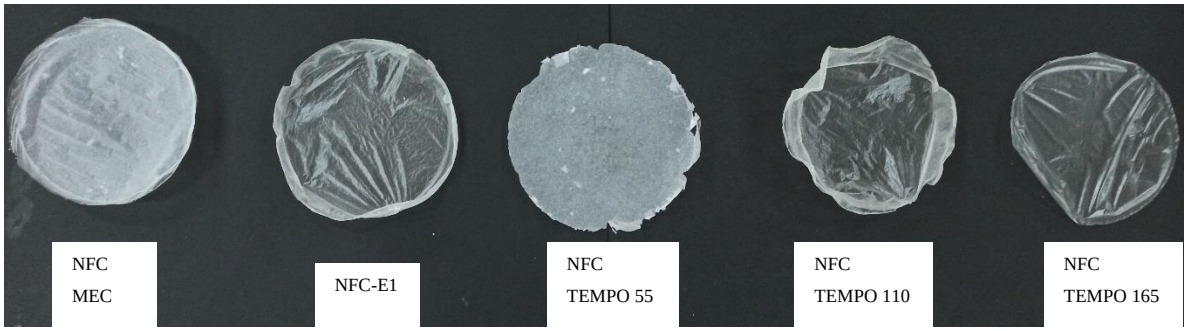

Figure 16a. NFC-only films, for all NFC samples (from left to right: NFC Mec, NFC-E1, NFC TEMPO 55, NFC TEMPO 110 and NFC TEMPO 165).

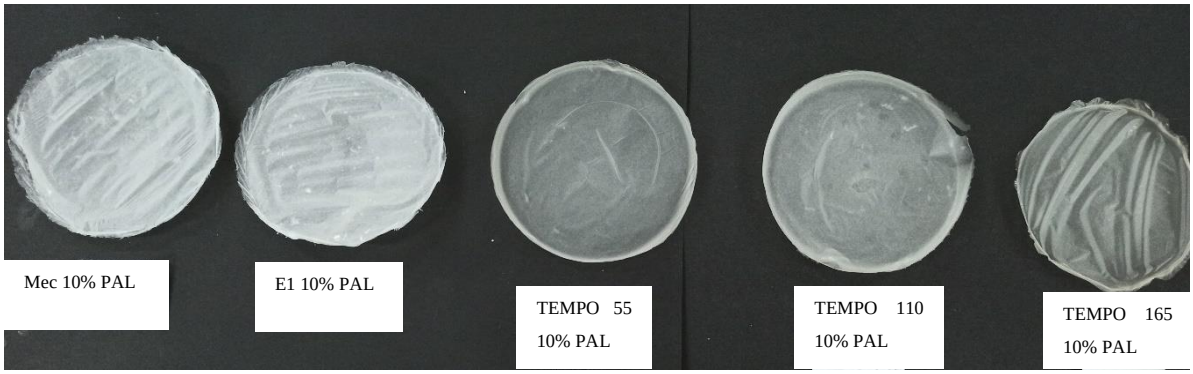

Figure 16b. Films with 10% PAL, for all NFC samples (from left to right: NFC Mec, NFC-E1, NFC TEMPO 55, NFC TEMPO 110 and NFC TEMPO 165).

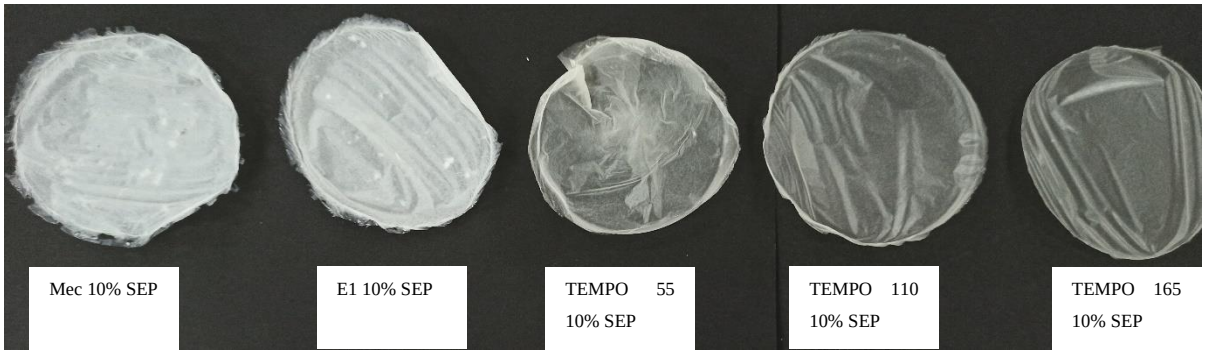

Figure 16c. Films with 10% SEP, for all NFC samples (from left to right: NFC Mec, NFC-E1, NFC TEMPO 55, NFC TEMPO 110 and NFC TEMPO 165).

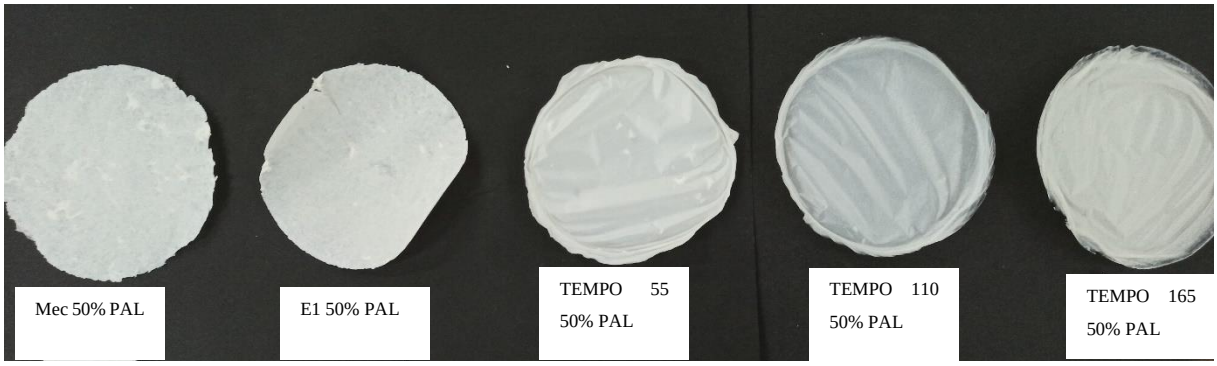

Figure 16d. Films with 50% PAL, for all NFC samples (from left to right: NFC Mec, NFC-E1, NFC TEMPO 55, NFC TEMPO 110 and NFC TEMPO 165).

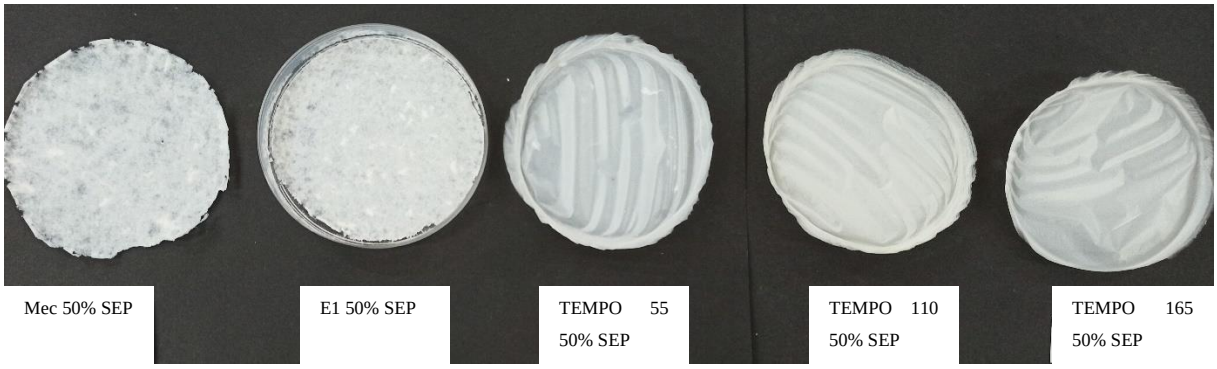

Figure 16e. Films with 50% SEP, for all NFC samples (from left to right: NFC Mec, NFC-E1, NFC TEMPO 55, NFC TEMPO 110 and NFC TEMPO 165).

Especially for NFC-only films (**Figure 16a**) and films with 10% mineral (**Figures 16b** and **16c**), the more the cellulose is fibrillated, the more transparent the film is. An exception to this trend is the NFC-only TEMPO 55 film, that exhibits fibre spots on the film surface, that could be associated with poor stability of the suspension after the homogenization. There is also a clear improvement when moving from the mechanical and enzymatic NFCs to the TEMPO-oxidized ones, particularly when incorporating 10% of mineral. These films (**Figures 16b** and **16c**) show very promising results since they achieved the desired transparency, as it is possible to see through them. Incorporating 50% of mineral in the films (**Figures 16d** and **16e**) makes them very opaque and rigid, massively lowering its resistance to touch.

Another technique used for the preparation of the films was vacuum filtration. This method allowed to prepare the films in a faster way, compared to the solvent casting approach, as it only required an overnight drying (either at room conditions or in the oven). The filtration process lasted for few minutes (*ca.* 2 minutes) for the mechanical and enzymatic suspensions, as they did not present a high viscosity, while for the TEMPO samples the time to filtrate them took a few hours (*ca.* 2 hours), due to the high viscosity exhibited by the suspensions. Since TEMPO samples were subjected to a severe vacuum for a long time, it became difficult to separate them from the filter paper, thus not being possible to test all of them at FFUC. The films that could be removed are exhibited in **Figure 17**.

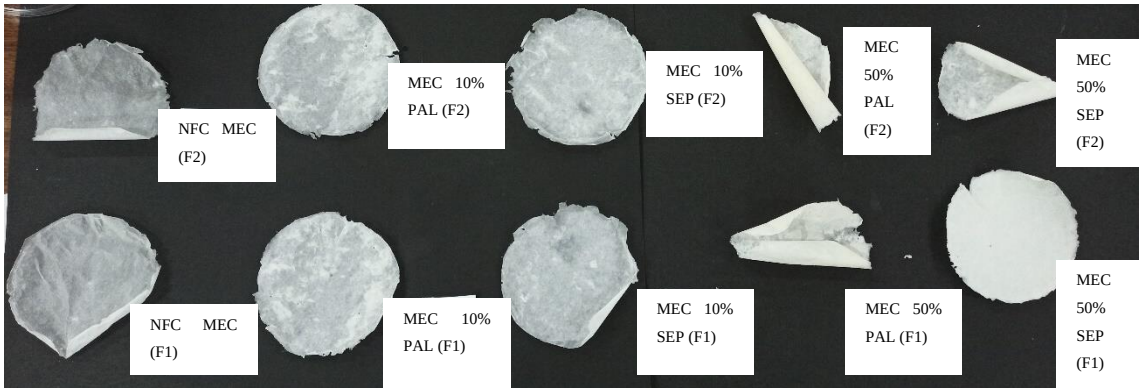

Figure 17a. Films obtained through vacuum filtration (F) and dried at room temperature (1) and in the oven at 50ºC (2), for NFC Mec.

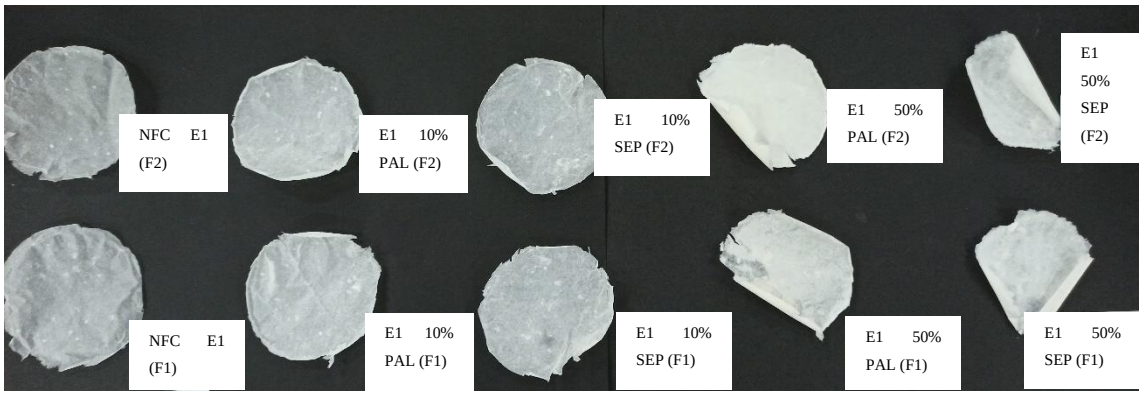

Figure 17b. Films obtained through vacuum filtration (F) and dried at room temperature (1) and in the oven at 50ºC (2), for NFC-E1.

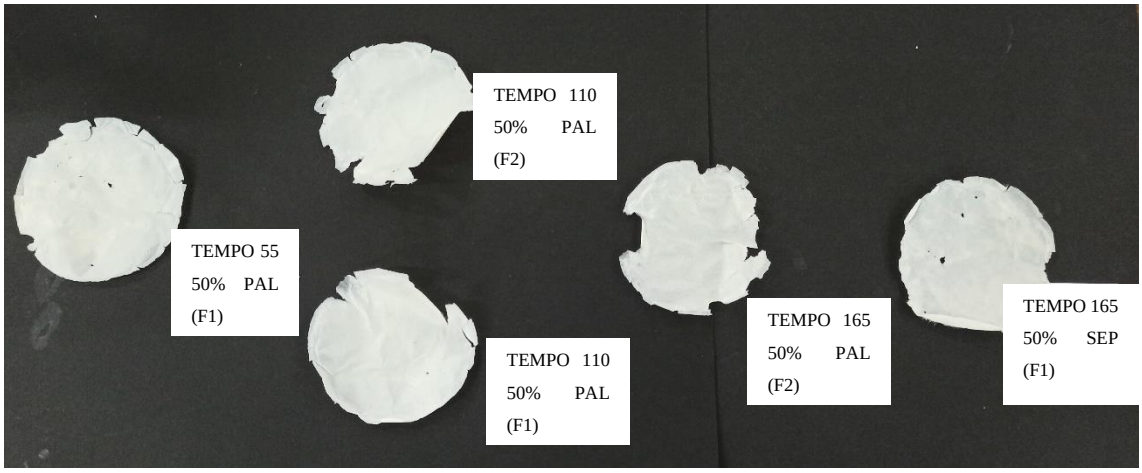

Figure 17c. Films obtained through vacuum filtration (F) and dried at room temperature (1) and in the oven at 50ºC (2), for NFC TEMPO 55, 110 and 165.

These films obtained from vacuum filtration presented smaller diameter, when compared to the ones obtained from solvent casting, due to the diameter of the filtration apparatus. Also, it was not observed visible differences between those left drying at room temperature and in the oven, with the latter ones only exhibiting a slightly increased wrinkling, caused by the forced drying. The incorporation of minerals made the films very fragile, hence the visible damage caused by its separation from the filter paper. However, despite the damage to the film's borders, as only a small 4x4 cm shape is required to ascertain their mechanical properties through the tests done at FFUC, these films were still viable to be tested.

Before proceeding to the mechanical tests, the thickness and light transmittance of the films were measured in an optical microscope and on a UV-Vis spectrophotometer, respectively, using very small strips, *ca*. 5 mm of width. An example of the thickness measurement is shown in **Figure 18**, where is possible to observe the cross-section of a thin NFC film.

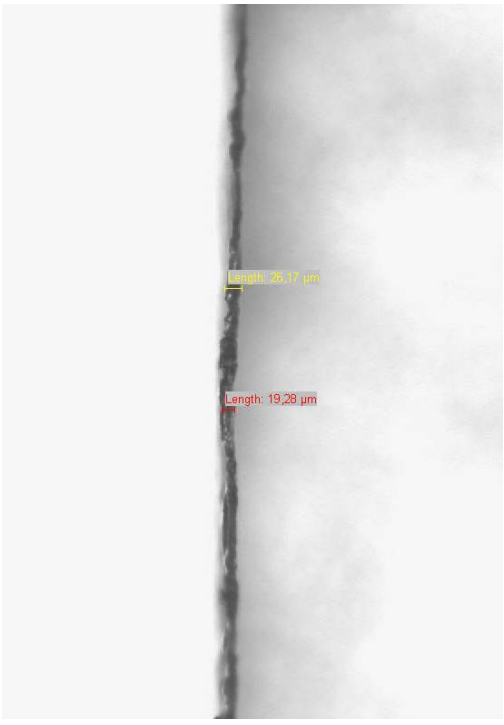

Figure 18. Microscope image of the cross-section of a NFC film for thickness measurement (NFC TEMPO 55), obtained through solvent casting.

Typically, two measurements were made in each film, in different sections of the strip, being then considered an average of these values. **Table 13** contains the average

values of the thickness of the several measured films, obtained using a solvent casting method.

Table 13. Average thickness, in μm, for the films obtained through solvent casting.

NFC Sample	Average film thickness (μm)				
	NFC only	10% PAL	10% SEP	50% PAL	50% SEP
Mec	24.1	26.2	36.5	22.0	24.8
Enzyme 1	16.5	17.9	28.2	25.5	-
TEMPO 55	22.7	17.6	17.2	24.8	24.1
TEMPO 110	19.9	19.9	20.7	23.4	22.7
TEMPO 165	22.7	16.5	28.9	21.1	19.9

From the results displayed in **Table 13**, it is possible to see that the solvent casting method allowed the preparation of films with low thickness. Those obtained from NFC-E1 showed the lowest thickness among the NFC only films, while those produced from NFC TEMPO 165 yielded the thinnest films when incorporating minerals (except with 10% SEP). Although it was not always the case, it was expected to have an increase in thickness when incorporating minerals, as the suspensions became denser.

In the films produced by filtration, when was possible to remove the filter paper, their thickness was also measured. Unfortunately, there was a significant amount of films whose thickness measurement was not feasible, especially those prepared from NFC TEMPO samples. The thickness of the films obtained from vacuum filtration is shown in **Table 14**.

Table 14a. Average thickness, in μm, for the films obtained through vacuum filtration, and dried at room temperature.

NFC Sample	Average film thickness (μm)				
	NFC only	10% PAL	10% SEP	50% PAL	50% SEP
Mec	22.0	24.8	20.0	29.6	30.3
Enzyme 1	31.0	26.2	22.7	31.7	31.7
TEMPO 55	24.1	-	21.4	25.5	31.7
TEMPO 110	-	-	16.5	22.7	26.2
TEMPO 165	-	-	-	27.5	18.6

Table 14b. Average thickness, in μm, for the films obtained through vacuum filtration, and dried in the oven at 50ºC.

NFC Sample	Average film thickness (μm)				
	NFC only	10% PAL	10% SEP	50% PAL	50% SEP
Mec	22.5	23.4	26.2	45.5	33.8
Enzyme 1	34.4	26.9	23.4	34.4	24.1
TEMPO 55	-	24.1	-	25.5	-
TEMPO 110	-	-	-	18.6	-
TEMPO 165	-	-	-	42.0	-

On most of the cases, the films obtained from vacuum filtration exhibit a higher thickness than those obtained from solvent casting. This was an expected result, since the dimensions of the filtration plaque were smaller than the Petri dish's, while the quantity of the suspension was the same for a smaller area, which would result in a higher thickness of the film. Values present in **Tables 14a** and **14b** show an increase in the films' thickness when incorporating minerals. Regarding the different minerals used, no clear trend concerning their influence in the films' thickness can be ascertained. However, it would be predictable that a difference between the two minerals would occur, as the PAL suspensions (1%, w/w) were somehow unstable, since there was a predisposition of the mineral to sediment in the bottom of the glass beaker, after high-speed homogenization.

Light transmittance (LT) was also determined, using a UV-Vis spectrophotometer, with a wavelength sweeping from 800nm to 200nm, at a speed of 400 nm/min. **Tables 15a** and **15b** show the maximum values of transmittance obtained, in the visible range (600nm), in %, for the samples that could be tested, for solvent casting and vacuum filtration films, respectively. For fully detailed spectra data, please see supplementary material (**Annex III**).

Table 15a. Light transmittance in the visible range (at 600nm), in %, for films obtained through solvent casting.

Film Sample	Light Transmittance at 600nm (%)

NFC Mec	NFC Only	9.8
	10% PAL	5.5
	10% SEP	3.5
	50% PAL	1.3
Enzyme 1	NFC Only	26.1
	10% PAL	4.9
TEMPO 55	NFC Only	10.0 *
	10% PAL	15.4
	10% SEP	62.1 *
	50% PAL	2.2
	50% SEP	8.3
TEMPO 110	NFC Only	35.1
	10% PAL	19.6
	10% SEP	38.4 *
	50% PAL	7.9
	50% SEP	3.0
TEMPO 165	NFC Only	44.6
	10% PAL	30.2
	50% PAL	2.0
	50% SEP	3.5

*these values were unexpected, and could be associated to difficulties in the preparation of the films, as well as in the measurement of LT.

Table 15b. Light transmittance in the visible range (at 600nm), in %, for films obtained through vacuum filtration and dried at room temperature (Batch 1) and in the oven at 50ºC (Batch 2).

Film Sample		Batch	Light Transmittance at 600nm (%)
NFC Mec	NFC Only	1	3.8
		2	5.4
	10% SEP	2	2.3
	50% PAL	2	0.7
	50% SEP	2	1.0
Enzyme 1	NFC Only	1	4.4

		2	4.4
	10% PAL	1	2.1
		2	3.5
	10% SEP	1	2.7
		2	2.8
	50% PAL	1	0.6
		2	0.5
	50% SEP	1	2.1
		2	0.7
TEMPO 110	50% PAL	1	0.6
	50% SEP	1	1.0
TEMPO 165	NFC Only	2	48.9
	50% PAL	2	1.2

Even though some films from **Figures 16** and **17** were completely see-through, the light transmittance was generally very low for most of them. TEMPO-oxidized NFCs exhibited the highest values for LT, which is according to what was previously mentioned, and in agreement with previous results (Coelho, 2016). Incorporating minerals caused a massive reduction on this parameter, since the films became progressively opaquer. However, when using 10% (w/w) of minerals, some good LT values were attained, with 19.6% and 30.2% for NFC TEMPO 110 and 165 films. Using 50% (w/w) of minerals in the preparation of the films, often led to a light transmittance below 2% for vacuum filtered films, while those obtained from solvent casting showed a tendency to have higher transparency, thus the higher LT values. With the results from **Table 15b**, it was not possible to establish any clear tendency between films left drying at room temperature and in the oven. When sweeping through UV wavelength, there was an abrupt drop of the LT values to almost 0%, starting at *ca*. 400nm.

The films were then subjected to a traction test (elongation at break), which gives the relationship between stress and strain, being an indicator of the stretching load force the material can take and the distance it stretches before failure. The operating conditions of the elongation at break test are given in **Figure 19**.

Caption	Value	Units
Test Mode	Tension	
Test Speed	0,50	mm/sec
Target Mode	Distance	
Distance	10,000	mm

Figure 19. Operating conditions used in the elongation at break test, set on the testing software.

As mentioned before, not all films obtained through vacuum filtration were tested, due to difficulties in removing the films from the filter paper. **Table 16** indicates the values of the load force and stretched distance, before failure, for the tested films.

Table 16a. Load force (N) and stretched distance (mm) before failure, for films obtained through solvent casting.

NFC Sample	Properties	NFC Only	10% PAL	10% SEP	50% PAL	50% SEP
Mec	F (N)	33.26	31.96	32.55	17.8	14.39
	ΔL (mm)	1.119	0.439	0.639	0.249	0.139
Enzyme 1	F (N)	46.99	39.25	19.00	-	-
	ΔL (mm)	0.799	0.846	0.739	-	-
TEMPO 55	F (N)	53.15	31.64	9.00	9.91	10.43
	ΔL (mm)	0.479	0.329	0.849	0.139	0.419
TEMPO 110	F (N)	48.56	22.91	30.82	26.57	14.25
	ΔL (mm)	1.239	0.249	0.349	0.379	0.369
TEMPO 165	F (N)	-	26.38	48.1	-	-
	ΔL (mm)	-	0.259	0.339	-	-

Table 16b. Load force (N) and stretching distance (mm) before failure, for films obtained through vacuum filtration and dried at room temperature (Batch 1) and in the oven at 50ºC (Batch 2).

NFC Sample	Batch	Properties	NFC Only	10% PAL	10% SEP	50% PAL	50% SEP

Mec	1	F (N)	73.91	-	61.83	-	13.99
		ΔL (mm)	1.159	-	1.199	-	0.299
	2	F (N)	62.08	-	67.16	35.52	30.25
		ΔL (mm)	1.179	-	1.229	0.629	0.939
Enzyme 1	1	F (N)	64.42	-	44.23	18.43	15.38
		ΔL (mm)	1.019	-	0.749	0.589	0.409
	2	F (N)	74.51	62.43	71.3	10.58	23.15
		ΔL (mm)	1.029	0.929	1.319	0.199	0.359
TEMPO 55	1	F (N)	-	-	-	-	45.02
		ΔL (mm)	-	-	-	-	0.509
	2	F (N)	-	-	-	-	-
		ΔL (mm)	-	-	-	-	-
TEMPO 110	1	F (N)	-	-	-	44.85	36.07
		ΔL (mm)	-	-	-	0.819	0.399
	2	F (N)	-	-	-	5.33	-
		ΔL (mm)	-	-	-	0.359	-
TEMPO 165	1	F (N)	65.04	-	-	36.77	-
		ΔL (mm)	0.879	-	-	0.529	-
	2	F (N)	-	-	-	-	30.61
		ΔL (mm)	-	-	-	-	0.349

Comparing films among the samples produced with the same NFC, there is a clear decrease in the load the films can take before failure as there is an increase in the mineral quantity. When observing the films from **Figures 16** and **17**, it was possible to verify the increase in its fragility, being very easy to rip them by applying very little strength. This has now been proven through the values of **Table 16**, as the load force is higher for NFC only films. Although very few films obtained through vacuum filtration were tested, there is an obvious improvement in their mechanical properties compared to those produced through solvent casting. The highest load force obtained for the films prepared from solvent casting was 53.15 N (TEMPO 55 without mineral) and was inferior to the lowest load obtained for a NFC-only film obtained from vacuum filtration (62.08 N for NFC Mec). Both films from NFC Mec and NFC-E1 yielded very promising results, even when small quantities of minerals were incorporated, though NFC TEMPO films exhibited the

most interesting results for higher mineral quantities, as a 50% film could stand up to a 44.85 N load before failure. The drying method also influenced the strain of the films before break, as those that were dried at an oven at 50ºC could resist, in general, until higher loads before failure, comparing to those dried at room temperature. All these results are in good agreement with results reported in literature (Alves *et al.*, 2019; Garusinghe *et al.*, 2018; Ho *et al.*, 2012), though all the films should have been tested, which was not possible.

To further evaluate the mechanical properties and measure the tensile stiffness of the films, the tensile strength, elongation at break, and Young's modulus (E) were determined, through **Equations 10**, **11** and **12**, and are expressed in **Table 17**, for the films whose both thickness and tensile properties have been measured. To exemplify the determination of this properties, a NFC-Mec film with an initial length (L_0) of 4 cm and a thickness of 24.1 μm will have a cross-sectional area (A) of 9.6 $x10^{-7}$ m^2, which leads to a tensile strength of 34.5 MPa, an elongation at break of 2.8% and a Young's modulus of 1.2 GPa.

Table 17a. Tensile strength (MPa), elongation at break (%) and Young's modulus (GPa), for films obtained through solvent casting.

NFC Sample		Tensile Strength (MPa)	Elongation at break (%)	E (GPa)
Mec	NFC Only	34.5	2.8	1.2
	10% PAL	30.5	1.1	2.8
	10% SEP	22.3	1.6	1.4
	50% PAL	20.2	0.6	3.2
	50% SEP	14.5	0.4	4.2
Enzyme 1	NFC Only	71.1	2.0	3.6
	10% PAL	54.8	2.1	2.6
	10% SEP	16.8	1.9	0.9
TEMPO 55	NFC Only	58.5	1.2	4.9
	10% PAL	45.0	0.8	5.5
	10% SEP	13.1	2.1	0.6
	50% PAL	10.0	0.4	2.9
	50% SEP	10.8	1.1	1.0

TEMPO 110	NFC Only	60.8	3.1	2.0
	10% PAL	28.7	0.6	4.6
	10% SEP	37.3	0.9	4.3
	50% PAL	28.4	1.0	3.0
	50% SEP	15.7	0.9	1.7
TEMPO 165	10% PAL	39.9	0.7	6.2
	10% SEP	44.8	0.9	5.3

Table 17b. Tensile strength (MPa), elongation at break (%), and Young's modulus for films obtained through vacuum filtration and dried at room temperature (Batch 1) and in the oven at 50ºC (Batch 2).

NFC Sample	Batch		Tensile Strength (MPa)	Elongation at break (%)	E (GPa)
Mec	1	NFC Only	83.9	2.9	2.9
	2		68.9	3.0	2.3
	1	10% SEP	77.4	3	2.6
	2		64.2	3.1	2.1
	2	50% PAL	17.9	1.6	1.1
	1	50% SEP	11.5	0.8	1.5
	2		22.4	2.4	1.0
Enzyme 1	1	NFC Only	52.0	2.6	2.0
	2		54.1	2.6	2.1
	2	10% PAL	58.1	2.3	2.5
	1	10% SEP	48.7	1.9	2.6
	2		76.1	3.3	2.3
	1	50% PAL	14.5	1.5	1.0
	2		7.7	0.5	1.5
	1	50% SEP	12.1	1.0	1.2
	2		24.0	0.9	2.7
TEMPO 55	1	50% SEP	35.5	1.3	2.8
TEMPO 110	1	50% PAL	49.3	2.1	2.4

	2		7.2	0.9	0.8
	1	50% SEP	34.5	1.0	3.5
TEMPO 165	1	50% PAL	33.4	1.3	2.5

Overall, tensile strength and elongation tend to decrease with the incorporation of minerals, making it more fragile. Results on **Table 17** corroborate the previously mentioned claim that films obtained from vacuum filtration exhibit, in general, better mechanical properties than those produced from solvent casting. A relationship between tensile strength (**Table 17**) and thickness (**Tables 13** and **14**) can also be established, with a clear improvement on the film's resistance for higher thicknesses.

Young's modulus indicates the stiffness of a material, with higher values corresponding to a stiffer and less elastic film. For NFC Mec prepared through solvent casting, there is a tendency to increase the Young's modulus values upon incorporation of minerals, associated with an increased stiffness of the material. However, high Young's modulus values for films with incorporated minerals are only observable with NFC TEMPO 110 and 165 filtered films, attaining values up to 3.5 GPa. Since this property is related to both strain and stress, it is expected to have lower Young's modulus values for the films that can suffer more stretching before failure, meaning they have a higher elasticity. Overall, there is no general tendency regarding the evolution of Young's modulus with the mineral increase, as, in some situations such as NFC-E1 filtered films, these values are very similar to each other.

5. Conclusions

Considering the purpose of this work, it is possible to claim that IGC poses as a very useful technique to ascertain the surface properties of NFCs, as it gives several details which could be useful to predict their compatibility with other materials, such as minerals. Using IGC, five different NFC samples were characterized, which allowed the comparison between the use of distinct pre-treatments for their production: mechanical, enzymatic and chemical (TEMPO). Palygorskite and sepiolite were also analysed through IGC.

The dispersive component of the surface energy (γ^{sd}), measured at 35ºC, 40ºC, 45ºC and 50ºC was in the range of 39.8 – 48.9 mJ.m^{-2} for NFC Mec, 34.3 – 36.7 mJ.m^{-2} for NFC TEMPO 55, 31.7 – 40.5 mJ.m^{-2} for NFC TEMPO 165, 36.2 – 42.7 mJ.m^{-2} for NFC-E1 and 37.1 – 40.4 mJ.m^{-2} for NFC-E2. Overall, γ^{sd} decreased with temperature, as expected, although at higher temperatures (50ºC) an increase was sometimes verified, that can be associated with minor changes in the sample's structure. NFC Mec exhibited the highest values for γ^{sd}, that are probably associated with its higher crystallinity than the remaining samples (>70% crystallinity). Between TEMPO-oxidized samples, it is possible to claim that the higher the fibrillation (higher quantity of added NaClO), the higher the dispersive component of the surface energy.

Regarding Lewis acid-base characteristics, the NFC samples tended to show greater affinity with amphoteric (acetone, ETA) and basic (THF, ethyl ether) probes, revealing a prevalence of the acidic character of the NFC's surface, which is also supported by the low interaction with acidic probes, such as TCM.

The specific component of the enthalpy (ΔH^{as}) and entropy (ΔS^{as}) of adsorption was also considered. However, since a good linear fit of $\Delta G^{as}/T$ vs. 1/T is required to obtain these parameters, it was not possible to draw any conclusions, as most of the samples showed a poor fitting with the several polar probes.

For mineral samples, the dispersive component of the surface energy was 115.9 mJ.m^{-2} and 83.4 mJ.m^{-2} for sepiolite and palygorskite samples, respectively. Higher γ^{sd} values indicate a higher tendency of the systems to undergo London and Debye interactions, thus a better compatibility with NFC is expected for films with incorporated sepiolite. Since no peaks or very insignificant signals were obtained upon injection of

polar probes, the Lewis acid-base character and the specific component of the enthalpy and entropy of adsorption were not assessed in this work.

The second stage of the current work consisted of preparing films using different ratios of minerals (0%, 10% and 50%, w/w). Suspensions of NFCs + minerals were weighed and homogenized, before preparing the films. Two different methods and sets of conditions were used to verify the difference in the obtained films, being these solvent casting and vacuum filtration, followed by drying at room temperature or in the oven at 50ºC.

Overall, the produced films showed good optical properties, although there were clear differences between them, whether caused by the NFC sample or the preparation method used. Films obtained from NFC Mec exhibited the highest opacity, even when no minerals were added. The improvement in the fibrillation yield, by introduction of an appropriate pre-treatment (enzymatic pre-treatment or TEMPO oxidation), in the NFC preparation, led to an obvious upturn of the film's transparency. It was possible to produce transparent films with 10% (w/w) minerals, especially for TEMPO 110 and TEMPO 165 NFCs. On the other hand, vacuum filtration led to films with smaller diameters, due to the smaller dimensions of the available filters, but allowed a much faster preparation of films (*ca*. 2 hours, instead of *ca.* 2 weeks required for the solvent casting method). There was a major difficulty associated with this method, caused by the use of severe vacuum, which made it impossible to remove the film from the filter paper without damaging it.

The thickness of the films was measured using a microscope, with values in the gamma of 22 – 45 μm for NFC Mec, 16 – 34 μm for NFC-E1, 17 – 32 μm for NFC TEMPO 55, 16 – 26 μm for NFC TEMPO 110 and 16 – 42 μm for NFC TEMPO 165. Films produced from vacuum filtration tended to have higher thicknesses, since the same suspension's quantity was added to a smaller area. Incorporating minerals was expected to lead to an increase in thickness, though that was not always verified, with some having small thickness even when adding 50% (w/w) minerals (19.9 μm for NFC TEMPO 165 with 50% SEP, for example). Higher thickness values were expected to be obtained, which leads to the conclusion that some material loss was experienced, as it has been previously reported in literature.

Light transmittance was also determined, using a spectrophotometer, and the results are accordingly to visual appearance. LT values were higher for films prepared

with only NFCs, progressively decreasing with the incorporation of minerals. With 10% PAL, it was possible to attain values of LT up to 30.2% (at 600nm), for those prepared through solvent casting, which makes this a promising technique to obtain very transparent films with addition of minerals. A conclusion of the effect of the drying method could not be reached, as there was no significant difference in LT values for the films left drying at room temperature or in the oven.

Films were also subjected to elongation at break tests, to assess the load they could take before failure, and establish comparisons with the amount of incorporated minerals, the preparation method and their thickness. It is possible to conclude that with vacuum filtration method, films tend to exhibit higher resistance to the applied tensions, which decreases with higher mineral quantities. Films obtained from solvent casting could endure up to a 53.15 N load, for a NFC TEMPO 55 film, while those produced from vacuum filtration could resist to a tension up to 74.51 N, for a NFC-E1 film. This difference was also verified when adding minerals, as the same films could take up to 14.25 N and 23.15 N, respectively, for NFC-E1 with 50% SEP. It can also be deduced that the drying method influences the mechanical properties of the film, since the films left drying at an oven tended to take a higher load before failure.

Tensile strength, elongation at break and Young's modulus were also determined, to establish a relationship between these properties and the film's mechanical resistance. NFC-Mec exhibited an increase in the Young's modulus from 1.2 GPa to 4.2 GPa upon incorporating minerals, associated with an increase in their stiffness. However, for films with 50% mineral, the highest achieved Young's modulus values were 3.5GPa for sepiolite, and 2.5 GPa for palygorskite, for filtered films. Other than these remarks, no clear trend was verified regarding the stiffness of the materials. As expected, films with a higher thickness could endure higher loads.

One can conclude that the best method to prepare films would be the vacuum filtration followed by forced drying at an oven. This method can be further improved, as will be described in the final chapter of this work, in order to prepare higher quality films and achieve better results, especially in terms of mechanical properties.

The current work was marked by constraints associated with COVID-19, especially regarding the time available to finish all the experimental work. Some other difficulties were also encountered throughout the work, such as the troublesome removal

of the films from the filter paper when using the vacuum filtration method, which limited the quality of the final results.

6. Future Prospects

To further develop the current work, based on what has already been done, a few suggestions are presented as follow:

- Analysis of replicas of the tested NFCs through IGC would be an interesting approach, to confirm the behaviour of the dispersive component of surface energy with temperature, as well as to try obtaining better linear fittings for the specific component of enthalpy and entropy of adsorption of polar probes. Similarly, replicas of palygorskite and sepiolite should also be analysed.
- The vacuum filtration process could be done at lower pH, to counter the difficulties encountered during filtration (TEMPO-oxidized NFC) and the separation of the film from the filter paper. Another promising alternative would be the use of a membrane filter, instead of the filter paper.
- Instead of using an oven at 50ºC, films could be dried using a hot press, to achieve better results regarding mechanical properties.
- Evaluating gas barrier properties, such as OTR and WVTR, would be an important step, as these are requirements for packaging and printed electronics uses.

7. Bibliography

Adscientis. (n.d.). *Surface Morphology*. Retrieved from https://www.adscientis.com/surface-morphology.html

Alves, L., Ferraz, E., & Gamelas, J. A. F. (2019). Composites of nanofibrillated cellulose with clay minerals: A review. *Advances in Colloid and Interface Science*, *272*. https://doi.org/10.1016/j.cis.2019.101994

Alves, L., Ferraz, E., Santarén, J., Rasteiro, M. G., & Gamelas, J. A. F. (2020). Improving Colloidal Stability of Sepiolite Suspensions: Effect of the Mechanical Disperser and Chemical Dispersant. *Minerals*, *10*(9), 779. https://doi.org/10.3390/min10090779

Arora, A., & Padua, G. W. (2010). Review: Nanocomposites in food packaging. *Journal of Food Science*, *75*(1). https://doi.org/10.1111/j.1750-3841.2009.01456.x

Aşkın, A., & Topaloğlu Yazıcı, D. (2005). Surface characterization of sepiolite by inverse gas chromatography. *Chromatographia*, *61*(11–12), 625–631. https://doi.org/10.1365/s10337-005-0558-z

ASTM International (2018). *Standard Test Method for Tensile Properties of Thin Plastic Sheeting*. Retrieved from https://www.astm.org/Standards/D882

Aulin, C., Salazar-Alvarez, G., & Lindström, T. (2012). High strength, flexible and transparent nanofibrillated cellulose-nanoclay biohybrid films with tunable oxygen and water vapor permeability. *Nanoscale*, *4*(20), 6622–6628. https://doi.org/10.1039/c2nr31726e

Bailey, S.W., & Brown. G. (1980). *Crystal Structures of Clay Minerals and their X-Ray Identification*. London, UK: Mineralogical Society.

Benítez, A. J., & Walther, A. (2017). Cellulose nanofibril nanopapers and bioinspired nanocomposites: A review to understand the mechanical property space. *Journal of Materials Chemistry A*, *5*(31), 16003–16024. https://doi.org/10.1039/c7ta02006f

Boudriche, L., Calvet, R., Hamdi, B., & Balard, H. (2012). Surface properties evolution of attapulgite by IGC analysis as a function of thermal treatment. *Colloids and Surfaces A: Physicochemical and Engineering Aspects*, *399*, 1–10. https://doi.org/10.1016/j.colsurfa.2012.02.015

Boudriche, L., Hamadi, B., Kessaïssia, Z., Calvet, R., Chamayou, A., Dodds, J. A., & Balard, H. (2010). An assessment of the surface properties of milled attapulgite using inverse gas chromatography. *Clays and Clay Minerals*, *58*(2), 143–153. https://doi.org/10.1346/CCMN.2010.0580201

Brigatti, M. F., Galán, E., & Theng, B. K. G. (2013). Structure and Mineralogy of Clay Minerals. *Developments in Clay Science*, *5*. https://doi.org/10.1016/B978-0-08-098258-8.00002-X

Brodin, F. W., Gregersen, Ø. W., & Syverud, K. (2014). Cellulose nanofibrils: Challenges and possibilities as a paper additive or coating material – A review. *Nordic Pulp & Paper Research Journal*, *29*(1), 156–166. https://doi.org/10.3183/npprj-2014-29-01-p156-166

Chen, Y., He, Y., Fan, D., Han, Y., Li, G., & Wang, S. (2017). An efficient method for cellulose nanofibrils length shearing via environmentally friendly mixed cellulase pretreatment. *Journal of Nanomaterials*, *2017*. https://doi.org/10.1155/2017/1591504

Coelho, M. V. (2016). *Filmes compósitos de celulose nanofibrilada e minerais argilosos* (Master Thesis). University of Coimbra, Faculty of Sciences and Technology, Portugal.

Eichhorn, S. J., Dufresne, A., Aranguren, M., Marcovich, N. E., Capadona, J. R., Rowan, S. J., … Peijs, T. (2010). Review: Current international research into cellulose nanofibres and nanocomposites. *Journal of Materials Science*, *45*. https://doi.org/10.1007/s10853-009-3874-0

Eriksen, Ø., Syverud, K., & Gregersen, Ø. (2008). The use of microfibrillated cellulose produced from kraft pulp as strength enhancer in TMP paper. *Nordic Pulp and Paper*

Research Journal, *23*(3), 299–304. https://doi.org/10.3183/npprj-2008-23-03-p299-304

Errokh, A., Magnin, A., Putaux, J. L., & Boufi, S. (2018). Morphology of the nanocellulose produced by periodate oxidation and reductive treatment of cellulose fibers. *Cellulose*, *25*(7), 3899–3911. https://doi.org/10.1007/s10570-018-1871-7

Fazeli, M., & Simão, R. A. (2019). Preparation and characterization of starch composites with cellulose nanofibers obtained by plasma treatment and ultrasonication. *Plasma Processes and Polymers*, *16*(6). https://doi.org/10.1002/ppap.201800167

Fukuzumi, H., Saito, T., Iwata, T., Kumamoto, Y., & Isogai, A. (2009). Transparent and high gas barrier films of cellulose nanofibers prepared by TEMPO-mediated oxidation. *Biomacromolecules*, *10*(1), 162–165. https://doi.org/10.1021/bm801065u

Gamelas, J. A. F. (2013). The surface properties of cellulose and lignocellulosic materials assessed by inverse gas chromatography: A review. *Cellulose*, *20*(6), 2675–2693. https://doi.org/10.1007/s10570-013-0066-5

Gamelas, J. A. F., & Ferraz, E. (2015). Composite films based on nanocellulose and nanoclay minerals as high strength materials with gas barrier capabilities: Key Points and Challenges. *BioResources*, *10*(4), 6310–6313. https://doi.org/10.15376/biores.10.4.6310-6313

Gamelas, J. A. F., Pedrosa, J., Lourenço, A. F., & Ferreira, P. J. (2015). Surface properties of distinct nanofibrillated celluloses assessed by inverse gas chromatography. *Colloids and Surfaces A: Physicochemical and Engineering Aspects*, *469*, 36–41. https://doi.org/10.1016/j.colsurfa.2014.12.058

Garusinghe, U. M., Varanasi, S., Raghuwanshi, V. S., Garnier, G., & Batchelor, W. (2018). Nanocellulose-montmorillonite composites of low water vapour permeability. *Colloids and Surfaces A: Physicochemical and Engineering Aspects*, *540*, 233–241. https://doi.org/10.1016/j.colsurfa.2018.01.010

Ghanadpour, M., Carosio, F., Ruda, M. C., & Wågberg, L. (2018). Tuning the Nanoscale Properties of Phosphorylated Cellulose Nanofibril-Based Thin Films to Achieve

Highly Fire-Protecting Coatings for Flammable Solid Materials. *ACS Applied Materials and Interfaces*, *10*(38), 32543–32555. https://doi.org/10.1021/acsami.8b10309

Govt. of South Australia. (n.d.). *Palygorskite*. Retrieved from https://energymining.sa.gov.au/minerals/mineral_commodities/palygorskite?fbclid=IwAR23zo4WqGskuTetLPNUCamC7EArgazZ8m9sFGN1j-3qpMJp-13JHSHmdGM

Guggenheim, S., & Krekeler, M. P. S. (2011). The structures and microtextures of the palygorskite-sepiolite group minerals. *Developments in Clay Science, 3,* 3-32. https://doi.org/10.1016/B978-0-444-53607-5.00001-3

Halász, I., & Heine, E. (1967). Simple Approximation for Pressure Correction Factor in Gas Chromatography. *Analytical Chemistry*, *39*(11), 1313. https://doi.org/10.1021/ac60255a003

Harvey, C. C., & Lagaly, G. (2013). Industrial Applications. *Developments in Clay Science, 5,* 451-490. *https*://doi.org/10.1016/B978-0-08-098259-5.00018-4

Ho, T. T. T., Abe, K., Zimmermann, T., & Yano, H. (2015). Nanofibrillation of pulp fibers by twin-screw extrusion. *Cellulose*, *22*(1), 421–433. https://doi.org/10.1007/s10570-014-0518-6

Ho, T. T. T., Zimmermann, T., Ohr, S., & Caseri, W. R. (2012). Composites of cationic nanofibrillated cellulose and layered silicates: Water vapor barrier and mechanical properties. *ACS Applied Materials and Interfaces*, *4*(9), 4832–4840. https://doi.org/10.1021/am3011737

Hosterman, J. W., & Patterson, S. H. (1992). Bentonite and fuller's earth resources of the United States. *US Geological Survey Professional Paper*, *1522*, 1–2. https://doi.org/10.3133/pp1522

Isogai, A., Saito, T., & Fukuzumi, H. (2011). TEMPO-oxidized cellulose nanofibers. *Nanoscale*, *3*(1), 71–85. https://doi.org/10.1039/c0nr00583e

Jastrzebski, Z. D. (1960). Nature and properties of engineering materials. *Journal of the Franklin Institute*, *269*(3), 247. https://doi.org/10.1016/0016-0032(60)90295-7

Jones, D., Ormondroyd, G. O., Curling, S. F., Popescu, C. M., & Popescu, M. C. (2017). Chemical compositions of natural fibres. *Advanced High Strength Natural Fibre Composites in Construction*. https://doi.org/10.1016/B978-0-08-100411-1.00002-9

Krekeler, M. P. S., & Guggenheim, S. (2008). Defects in microstructure in palygorskite-sepiolite minerals: A transmission electron microscopy (TEM) study. *Applied Clay Science*, *39*(1–2), 98–105. https://doi.org/10.1016/j.clay.2007.05.001

L. Segal, J.J. Creely, A.E. Martin., & C.M. Conrad. (1959). An Empirical Method for Estimating the Degree of Crystallinity of Native Cellulose Using the X-Ray Diffractometer. *Textile Research Journal*, *29*(10), 786-794. https://doi.org/10.1177/004051755902901003

Lavoine, N., Desloges, I., Dufresne, A., & Bras, J. (2012). Microfibrillated cellulose - Its barrier properties and applications in cellulosic materials: A review. *Carbohydrate Polymers*, *90*(2), 735–764. https://doi.org/10.1016/j.carbpol.2012.05.026

Lazarević, S., Radovanović, Ž., Veljović, D., Onjia, A., Janaćković, D., & Petrović, R. (2009). Characterization of sepiolite by inverse gas chromatography at infinite and finite surface coverage. *Applied Clay Science*, *43*(1), 41–48. https://doi.org/10.1016/j.clay.2008.07.013

Liimatainen, H., Visanko, M., Sirviö, J. A., Hormi, O. E. O., & Niinimaki, J. (2012). Enhancement of the nanofibrillation of wood cellulose through sequential periodate-chlorite oxidation. *Biomacromolecules*, *13*(5), 1592–1597. https://doi.org/10.1021/bm300319m

Liu, Y., Gordeyeva, K., & Bergström, L. (2017). Steady-shear and viscoelastic properties of cellulose nanofibril–nanoclay dispersions. *Cellulose*, *24*(4), 1815–1824. https://doi.org/10.1007/s10570-017-1211-3

Liu, Y., Zhang, S., Wang, X., Pan, Y., Zhang, F., & Huang, J. (2020). Mechanical and aging resistance properties of polypropylene (PP) reinforced with

nanocellulose/attapulgite composites (NCC/AT). *Composite Interfaces*, *27*(1), 73–85. https://doi.org/10.1080/09276440.2019.1600971

Lourenço, A. F., Gamelas, J. A. F., Nunes, T., Amaral, J., Mutjé, P., & Ferreira, P. J. (2017). Influence of TEMPO-oxidised cellulose nanofibrils on the properties of filler-containing papers. *Cellulose*, *24*(1), 349–362. https://doi.org/10.1007/s10570-016-1121-9

Lourenço, A. F., Gamelas, J. A. F., Sarmento, P., & Ferreira, P. J. T. (2019). Enzymatic nanocellulose in papermaking – The key role as filler flocculant and strengthening agent. *Carbohydrate Polymers*, *224*(August), 115200. https://doi.org/10.1016/j.carbpol.2019.115200

Lu, X. (2019). Cellulose nanocrystals for wrinkled fabric. *BioResources*, *14*(4), 7632–7635. Retrieved from https://bioresources.cnr.ncsu.edu/resources/cellulose-nanocrystals-for-wrinkled-fabric/

Milczewska, K., & Voelkel, A. (2012). Inverse Gas Chromatography in Characterization of Composites Interaction. *Advanced Gas Chromatography - Progress in Agricultural, Biomedical and Industrial Applications*. https://doi.org/10.5772/32444

Miles, W. J. (2011). Amargosa sepiolite and saponite: Geology, mineralogy, and markets. *Developments in Clay Science*, *3*. https://doi.org/10.1016/B978-0-444-53607-5.00011-6

Millot, G. (1972). Geology of clays. *Geochimica et Cosmochimica Acta*, *36*, 103-104. https://doi.org/10.1016/0016-7037(72)90125-1

Naderi, A., Lindström, T., & Sundström, J. (2015). Repeated homogenization, a route for decreasing the energy consumption in the manufacturing process of carboxymethylated nanofibrillated cellulose?. *Cellulose*, *22*(2), 1147–1157. https://doi.org/10.1007/s10570-015-0576-4

Nelson, K., Retsina, T., Iakovlev, M., van Heiningen, A., Deng, Y., Shatkin, J. A., & Mulyadi, A. (2016). American process: Production of low cost nanocellulose for

renewable, advanced materials applications. *Springer Series in Materials Science*, *224*. https://doi.org/10.1007/978-3-319-23419-9_9

Nelson, S. A. (2015). *Phyllosilicates (Sheet Silicates)*. Retrieved from https://www.tulane.edu/~sanelson/eens211/phyllosilicates.htm

Rol, F., Saini, S., Meyer, V., Petit-Conil, M., & Bras, J. (2019). Production of cationic nanofibrils of cellulose by twin-screw extrusion. *Industrial Crops and Products*, *137*, 81–88. https://doi.org/10.1016/j.indcrop.2019.04.031

Shi, B. (2019). Problem in the molecular area of polar probe molecules used in inverse gas chromatography. *Journal of Chromatography A*, *1601*, 385–387. https://doi.org/10.1016/j.chroma.2019.05.027

Siemann, U. (2005). Solvent cast technology - A versatile tool for thin film production. *Progress in Colloid and Polymer Science*, *130*, 1–14. https://doi.org/10.1007/b107336

Tayeb, A. H., & Tajvidi, M. (2019). Sustainable Barrier System via Self-Assembly of Colloidal Montmorillonite and Cross-linking Resins on Nanocellulose Interfaces. *ACS Applied Materials and Interfaces*, *11*(1), 1604–1615. https://doi.org/10.1021/acsami.8b16659

Thielemans, W., Warbey, C. R., & Walsh, D. A. (2009). Permselective nanostructured membranes based on cellulose nanowhiskers. *Green Chemistry*, *11*(4), 531–553. https://doi.org/10.1039/b818056c

Tibolla, H., Pelissari, F. M., Rodrigues, M. I., & Menegalli, F. C. (2017). Cellulose nanofibers produced from banana peel by enzymatic treatment: Study of process conditions. *Industrial Crops and Products*, *95*, 664–674. https://doi.org/10.1016/j.indcrop.2016.11.035

Wang, C., Shi, J., He, M., Ding, L., Li, S., Wang, Z., & Wei, J. (2018). High strength cellulose/ATT composite films with good oxygen barrier property for sustainable packaging applications. *Cellulose*, *25*(7), 4145–4154. https://doi.org/10.1007/s10570-018-1855-7

Wang, W., & Wang, A. (2016). Recent progress in dispersion of palygorskite crystal bundles for nanocomposites. *Applied Clay Science*, *119*, 18–30. https://doi.org/10.1016/j.clay.2015.06.030

Wang, W., Sabo, R. C., Mozuch, M. D., Kersten, P., Zhu, J. Y., & Jin, Y. (2015). Physical and Mechanical Properties of Cellulose Nanofibril Films from Bleached Eucalyptus Pulp by Endoglucanase Treatment and Microfluidization. *Journal of Polymers and the Environment*, *23*(4), 551–558. https://doi.org/10.1007/s10924-015-0726-7

Wei, H., Rodriguez, K., Renneckar, S., & Vikesland, P. J. (2014). Environmental science and engineering applications of nanocellulose-based nanocomposites. *Environmental Science: Nano*, *1*(4), 302–316. https://doi.org/10.1039/c4en00059e

Wicklein, B., Kocjan, D., Carosio, F., Camino, G., & Bergström, L. (2016). Tuning the Nanocellulose-Borate Interaction to Achieve Highly Flame Retardant Hybrid Materials. *Chemistry of Materials*, *28*(7), 1985–1989. https://doi.org/10.1021/acs.chemmater.6b00564

Wu, C. N., Saito, T., Fujisawa, S., Fukuzumi, H., & Isogai, A. (2012). Ultrastrong and high gas-barrier nanocellulose/clay-layered composites. *Biomacromolecules*, *13*(6), 1927–1932. https://doi.org/10.1021/bm300465d

Wu, C. N., Yang, Q., Takeuchi, M., Saito, T., & Isogai, A. (2014). Highly tough and transparent layered composites of nanocellulose and synthetic silicate. *Nanoscale*, *6*(1), 392–399. https://doi.org/10.1039/c3nr04102f

Xie, H., Du, H., Yang, X., & Si, C. (2018). Recent Strategies in Preparation of Cellulose Nanocrystals and Cellulose Nanofibrils Derived from Raw Cellulose Materials. *International Journal of Polymer Science*, *2018*, 10–17. https://doi.org/10.1155/2018/7923068

Yang, Z., Peng, H., Wang, W., & Liu, T. (2010). Crystallization behavior of poly(ε-caprolactone)/layered double hydroxide nanocomposites. *Journal of Applied Polymer Science*, *116*(5), 2658–2667. https://doi.org/10.1002/app

Yuan, Z., Wei, W., & Wen, Y. (2019). Improving the production of nanofibrillated cellulose from bamboo pulp by the combined cellulase and refining treatment. *Journal of Chemical Technology and Biotechnology*, *94*(7), 2178–2186. https://doi.org/10.1002/jctb.5998

Zafar, R., Zia, K. M., Tabasum, S., Jabeen, F., Noreen, A., & Zuber, M. (2016). Polysaccharide based bionanocomposites, properties and applications: A review. *International Journal of Biological Macromolecules*, *92*, 1012–1024. https://doi.org/10.1016/j.ijbiomac.2016.07.102

Annex I – Packed Quantities

Table I. Packed masses (g) for all sample in IGC analysis.

Sample	Packed mass (g)
SEP	2.33
PAL	2.47
NFC Mec	1.97
NFC TEMPO 55	2.32
NFC TEMPO 110	1.91
NFC E1	1.81
NFC E2	3.92

Annex II – Suspensions for NFC-based films

Table II.1. Weighed quantities of suspensions for NFC-based films prepared from solvent casting, with 10% sepiolite (SEP) and palygorskite (PAL).

Consistency (%)	Mec		TEMPO 55		TEMPO 110		TEMPO 165		Enzyme 1	
	0.74		0.9		0.93		0.99		0.94	
	SEP	PAL	SEP	PAL	SEP	PAL	SEP	PAL	SEP	PAL
Mass (NFC suspension) (g)	11.384	11.359	11.165	11.161	11.162	11.163	11.160	11.164	11.162	11.163
Mass (NFC + mineral) (g)	12.412	12.419	12.423	12.400	12.423	12.416	12.422	12.423	12.418	12.407
Mass (mineral suspension) (g)	1.028	1.060	1.258	1.240	1.262	1.254	1.262	1.259	1.256	1.244
Mass (distilled water) (g)	47.622	47.598	47.613	47.715	47.587	47.660	47.730	47.580	47.596	47.635
Mass (total) (g)	60.034	60.017	60.036	60.115	60.011	60.076	60.152	60.003	60.014	60.041
Mass (NFC) (g)	0.084	0.084	0.100	0.100	0.104	0.104	0.110	0.111	0.105	0.105
Mass (mineral) (g)	0.010	0.011	0.013	0.012	0.013	0.013	0.013	0.013	0.013	0.012
Mass (total) (g)	0.095	0.095	0.113	0.113	0.116	0.116	0.123	0.123	0.117	0.117
% (NFC)	89.12	88.80	88.88	89.02	89.16	89.23	89.75	89.77	89.31	89.40
% (mineral)	10.88	11.20	11.12	10.98	10.84	10.77	10.25	10.23	10.69	10.60

Table II.2. Weighed quantities of suspensions for NFC-based films prepared from solvent casting, with 50% sepiolite (SEP) and palygorskite (PAL).

Consistency (%)	Mec		TEMPO 55		TEMPO 110		TEMPO 165		Enzyme 1	
	0.74		0.9		0.93		0.99		0.94	
	SEP	PAL	SEP	PAL	SEP	PAL	SEP	PAL	SEP	PAL
Mass (NFC suspension) (g)	7.130	7.120	6.396	6.403	6.530	6.894	6.252	6.214	6.546	6.537
Mass (NFC + mineral) (g)	12.429	12.402	12.404	12.409	12.461	12.404	12.456	12.412	12.421	12.432
Mass (mineral suspension) (g)	5.299	5.282	6.008	6.005	5.931	5.511	6.204	6.197	5.876	5.895
Mass (distilled water) (g)	47.665	47.625	47.685	47.616	47.571	47.658	47.663	47.632	47.627	47.758
Mass (total) (g)	60.094	60.027	60.089	60.024	60.032	60.063	60.119	60.043	60.048	60.189
Mass (NFC) (g)	0.053	0.053	0.058	0.058	0.061	0.064	0.062	0.062	0.062	0.061
Mass (mineral) (g)	0.053	0.053	0.060	0.060	0.059	0.055	0.062	0.062	0.059	0.059
Mass (total) (g)	0.106	0.106	0.118	0.118	0.120	0.119	0.124	0.123	0.120	0.120
%NFC	49.89	49.94	48.93	48.97	50.59	53.78	49.94	49.82	51.15	51.04
% mineral	50.00	50.06	51.07	51.03	49.41	46.22	50.06	50.18	48.85	48.96

Table II.3. Weighed quantities of suspensions for NFC-based films prepared from vacuum filtration, with 10% Sepiolite.

Consistency (%)	Mec		TEMPO 55		TEMPO 110		TEMPO 165		Enzyme 1	
	0.74		0.9		0.93		0.99		0.94	
	Air-dried	Oven-dried	Air-dried	Oven-dried	Air-dried	Oven-dried	Air-dried	Oven-dried	Air-dried	Oven-dried
Mass (NFC suspension) (g)	11.480	11.468	11.271	11.268	11.246	11.236	11.168	11.177	11.239	11.223
Mass (NFC + mineral) (g)	12.422	12.425	12.431	12.442	12.413	12.412	12.403	12.405	12.443	12.416
Mass (mineral suspension) (g)	0.942	0.957	1.160	1.174	1.167	1.176	1.235	1.228	1.204	1.193
Mass (distilled water) (g)	47.637	47.827	47.869	47.648	47.713	47.626	47.610	47.666	47.572	47.609
Mass (total) (g)	60.059	60.252	60.299	60.090	60.126	60.038	60.013	60.072	60.015	60.025
Mass (NFC) (g)	0.085	0.085	0.101	0.101	0.105	0.104	0.111	0.111	0.106	0.105
Mass (mineral) (g)	0.009	0.010	0.012	0.012	0.012	0.012	0.012	0.012	0.012	0.012
Mass (total) (g)	0.094	0.094	0.113	0.113	0.116	0.116	0.123	0.123	0.118	0.117
% NFC	90.0	89.9	89.7	89.6	90.0	89.9	89.9	90.0	89.8	89.8
% Mineral	10.0	10.1	10.3	10.4	10.0	10.1	10.1	10.0	10.2	10.2

Table II.4. Weighed quantities of suspensions for NFC-based films prepared from vacuum filtration, with 10% Palygorskite.

Consistency (%)	Mec 0.74		TEMPO 55 0.9		TEMPO 110 0.93		TEMPO 165 0.99		Enzyme 1 0.94	
	Air-dried	Oven-dried	Air-dried	Oven-dried	Air-dried	Oven-dried	Air-dried	Oven-dried	Air-dried	Oven-dried
Mass (NFC suspension) (g)	11.463	11.469	11.273	11.277	11.244	11.234	11.173	11.178	11.241	11.229
Mass (NFC + mineral) (g)	12.498	12.410	12.436	12.439	12.410	12.403	12.409	12.398	12.433	12.429
Mass (mineral suspension) (g)	1.035	0.941	1.162	1.162	1.166	1.169	1.235	1.220	1.192	1.200
Mass (distilled water) (g)	47.549	47.723	47.586	47.586	48.032	47.694	47.887	47.713	47.573	47.676
Mass (total) (g)	60.048	60.134	58.484	60.025	60.442	60.098	60.296	60.111	60.006	60.105
Mass (NFC) (g)	0.085	0.085	0.101	0.101	0.105	0.104	0.111	0.111	0.106	0.106
Mass (mineral) (g)	0.010	0.009	0.012	0.012	0.012	0.012	0.012	0.012	0.012	0.012
Mass (total) (g)	0.095	0.094	0.113	0.113	0.116	0.116	0.123	0.123	0.118	0.118
%NFC	89.1	90.0	89.7	89.7	90.0	89.9	90.0	90.1	89.9	89.8
% mineral	10.9	10.0	10.3	10.3	10.0	10.1	10.0	9.9	10.1	10.2

Table II.5. Weighed quantities of suspensions for NFC-based films prepared from vacuum filtration, with 50% Sepiolite.

Consistency (%)	Mech 0.74		TEMPO 55 0.9		TEMPO 110 0.93		TEMPO 165 0.99		Enzyme 1 0.94	
	Air-dried	Oven-dried	Air-dried	Oven-dried	Air-dried	Oven-dried	Air-dried	Oven-dried	Air-dried	Oven-dried
Mass (NFC suspension) (g)	7.139	7.141	6.539	6.526	6.420	6.418	6.234	6.226	6.392	6.386
Mass (NFC + mineral) (g)	12.392	12.422	12.424	12.439	12.436	12.431	12.390	12.403	12.405	12.423
Mass (mineral suspension) (g)	5.254	5.282	5.885	5.913	6.016	6.013	6.156	6.176	6.014	6.037
Mass (distilled water) (g)	47.659	47.670	47.844	47.664	47.595	47.582	47.735	47.888	47.688	47.564
Mass (total) (g)	60.051	60.092	60.268	60.103	60.031	60.013	60.125	60.291	60.093	59.986
Mass (NFC) (g)	0.053	0.053	0.059	0.059	0.060	0.060	0.062	0.062	0.060	0.060
Mass (mineral) (g)	0.053	0.053	0.059	0.059	0.060	0.060	0.062	0.062	0.060	0.060
Mass (total) (g)	0.105	0.106	0.118	0.118	0.120	0.120	0.123	0.123	0.120	0.120
%NFC	50.1	50.0	50.0	49.8	49.8	49.8	50.1	50.0	50.0	49.9
% mineral	49.9	50.0	50.0	50.2	50.2	50.2	49.9	50.0	50.0	50.1

Table III.5. Weighed quantities of suspensions for NFC-based films prepared from vacuum filtration, with 50% Palygorskite.

Consistency (%)	Mech 0.74		TEMPO 55 0.9		TEMPO 110 0.93		TEMPO 165 0.99		Enzyme 1 0.94	
	Air-dried	Oven-dried	Air-dried	Oven-dried	Air-dried	Oven-dried	Air-dried	Oven-dried	Air-dried	Oven-dried
Mass (NFC suspension) (g)	7.133	7.136	6.536	6.535	6.422	6.424	6.227	6.226	6.377	6.391
Mass (NFC + mineral) (g)	12.397	12.427	12.414	12.413	12.407	12.391	12.396	12.405	12.357	12.396
Mass (mineral suspension) (g)	5.264	5.291	5.878	5.878	5.985	5.967	6.169	6.179	5.981	6.006
Mass (distilled water) (g)	48.088	48.528	47.966	47.623	47.159	45.466	47.608	47.717	47.516	47.989
Mass (total) (g)	60.485	60.955	60.379	60.037	59.566	57.857	60.004	60.121	59.873	60.385
Mass (NFC) (g)	0.053	0.053	0.059	0.059	0.060	0.060	0.062	0.062	0.060	0.060
Mass (mineral) (g)	0.053	0.053	0.059	0.059	0.060	0.060	0.062	0.062	0.060	0.060
Mass (total) (g)	0.105	0.106	0.118	0.118	0.120	0.119	0.123	0.123	0.120	0.120
%Nfc	50.1	50.0	50.0	50.0	49.9	50.0	50.0	49.9	50.1	50.0
% Mineral	49.9	50.0	50.0	50.0	50.1	50.0	50.0	50.1	49.9	50.0

Annex III – Light Transmittance of NFC-based films

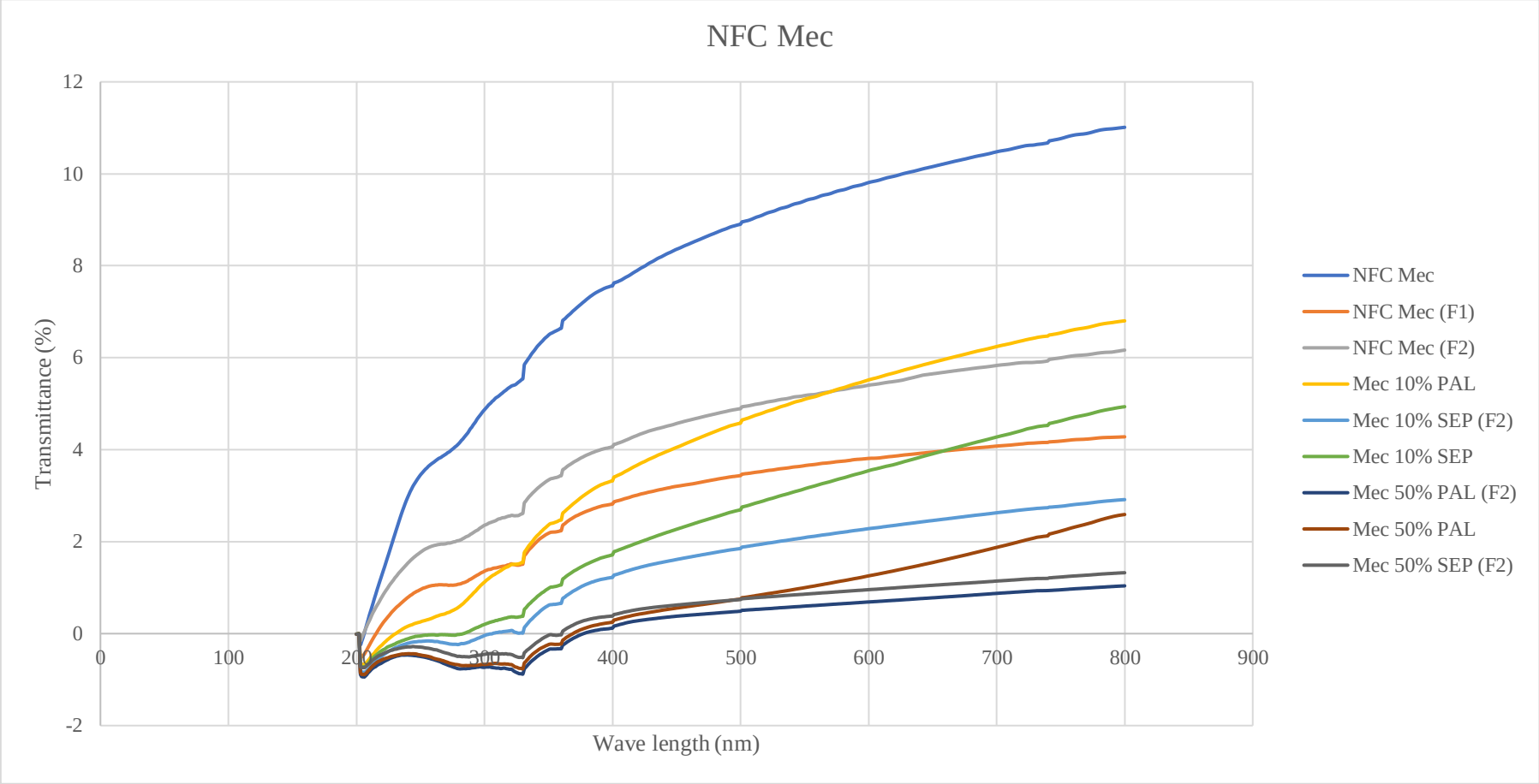

Figure III.1. Light transmittance for NFC Mec sample, for films obtained through solvent casting (-) and vacuum filtration (F1 – dried at room temperatures; F2 – dried in the oven at 50ºC).

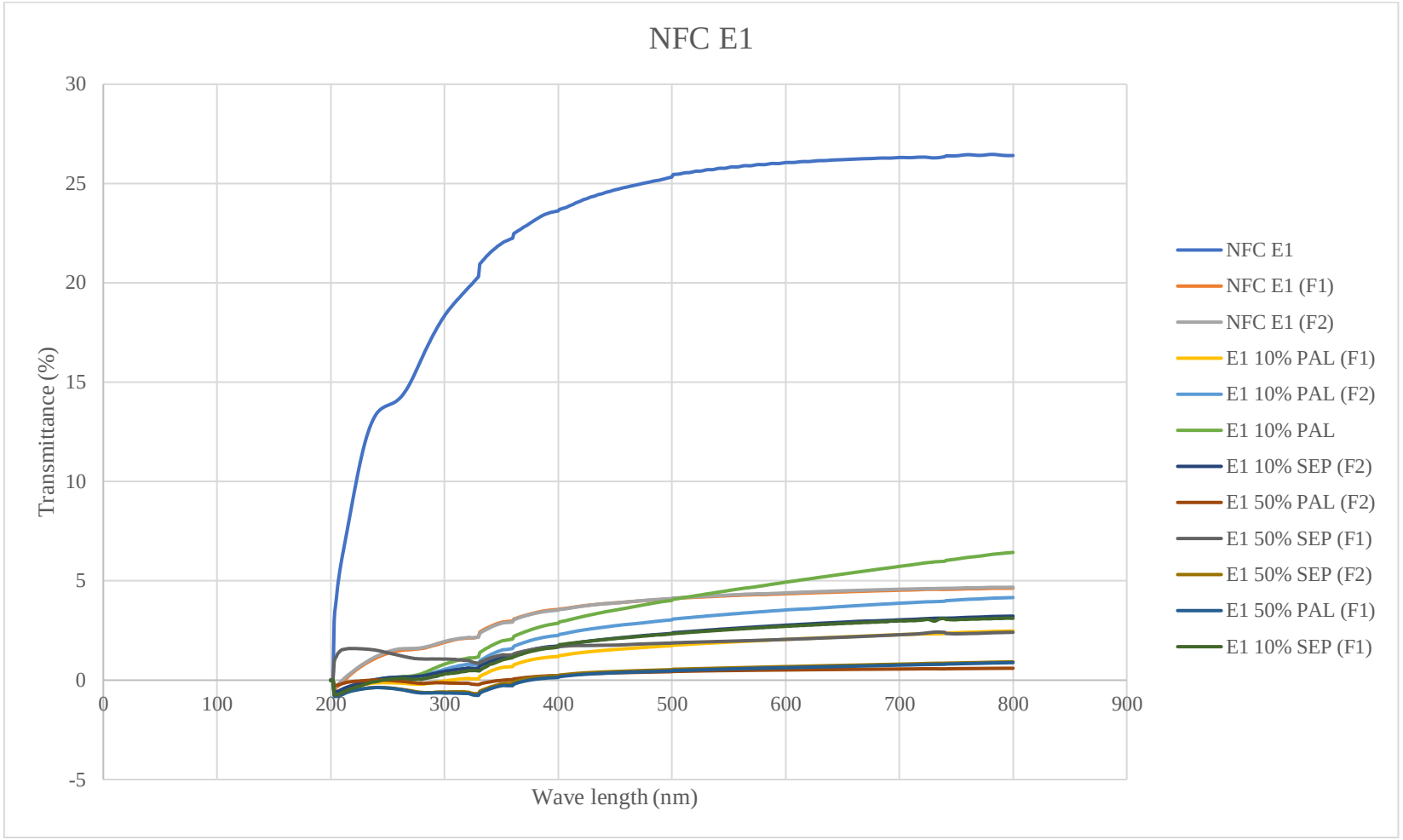

Figure III.2. Light transmittance for NFC E1 sample, for films obtained through solvent casting (-) and vacuum filtration (F1 – dried at room temperatures; F2 – dried in the oven at 50ºC).

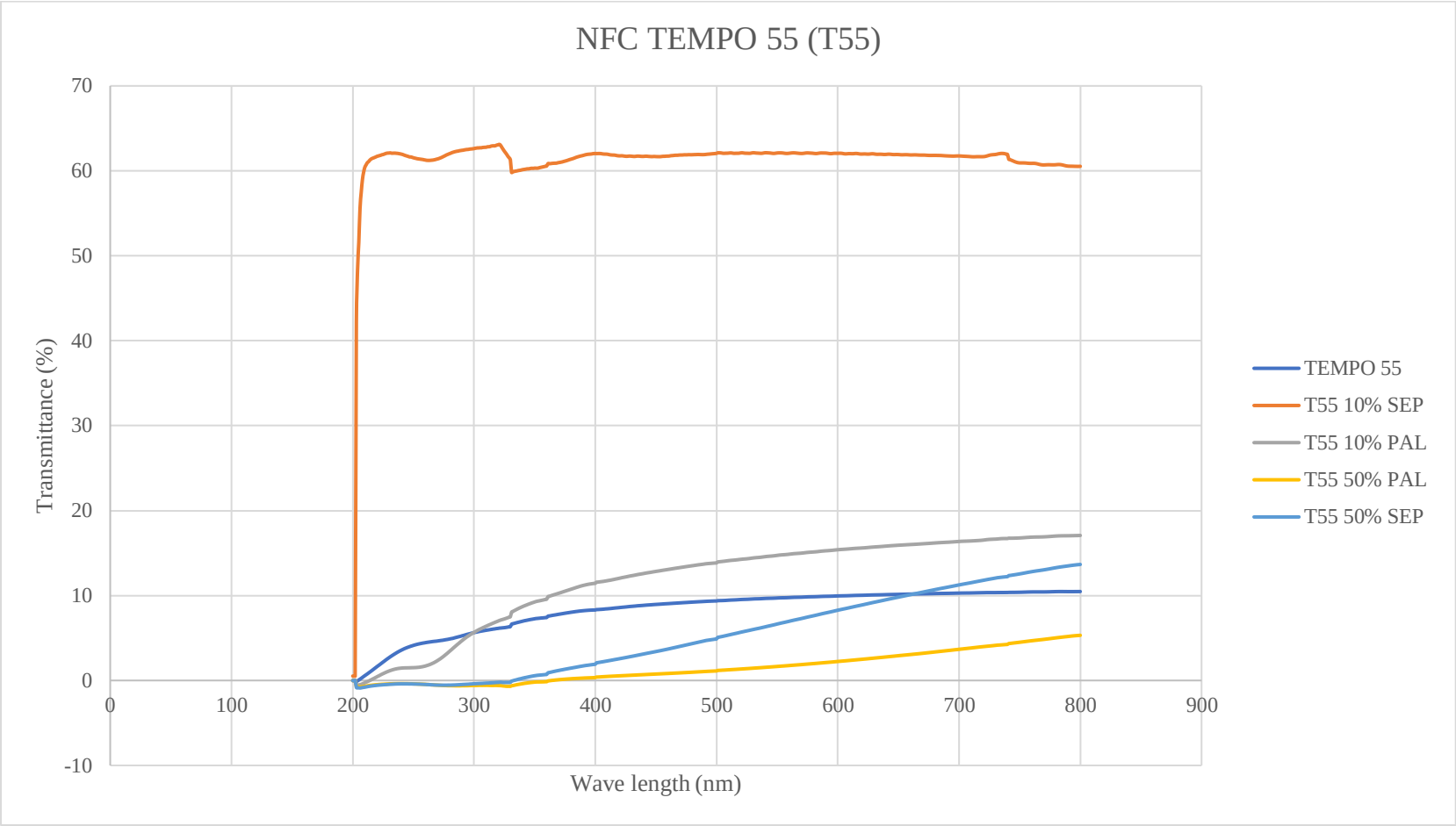

Figure III.3. Light transmittance for NFC TEMPO 55 sample (T55), for films obtained through solvent casting.

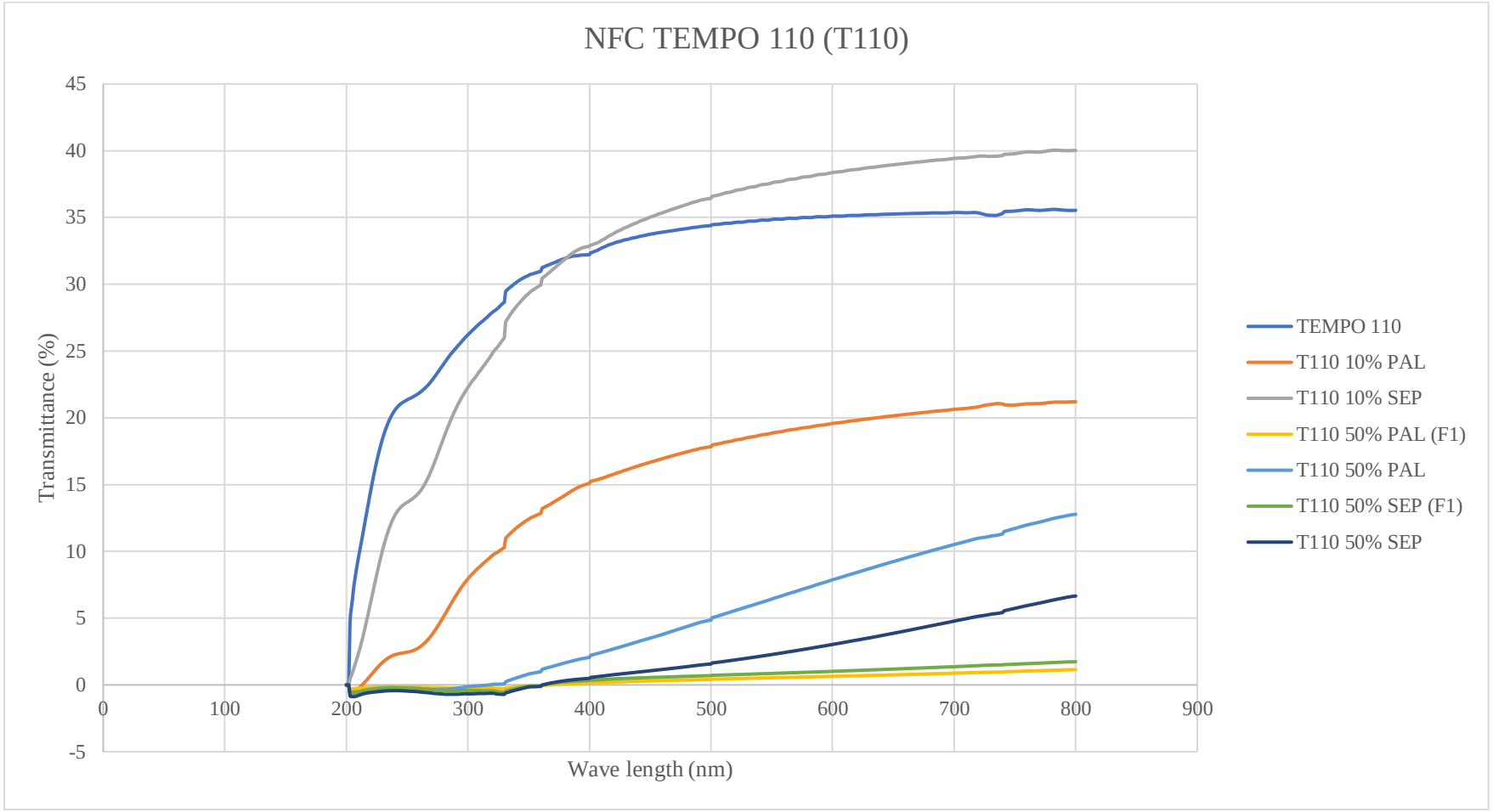

Figure III.4. Light transmittance for NFC TEMPO 110 sample (T110), for films obtained through solvent casting (-) and vacuum filtration (F1 – dried at room temperatures; F2 – dried in the oven at 50ºC).

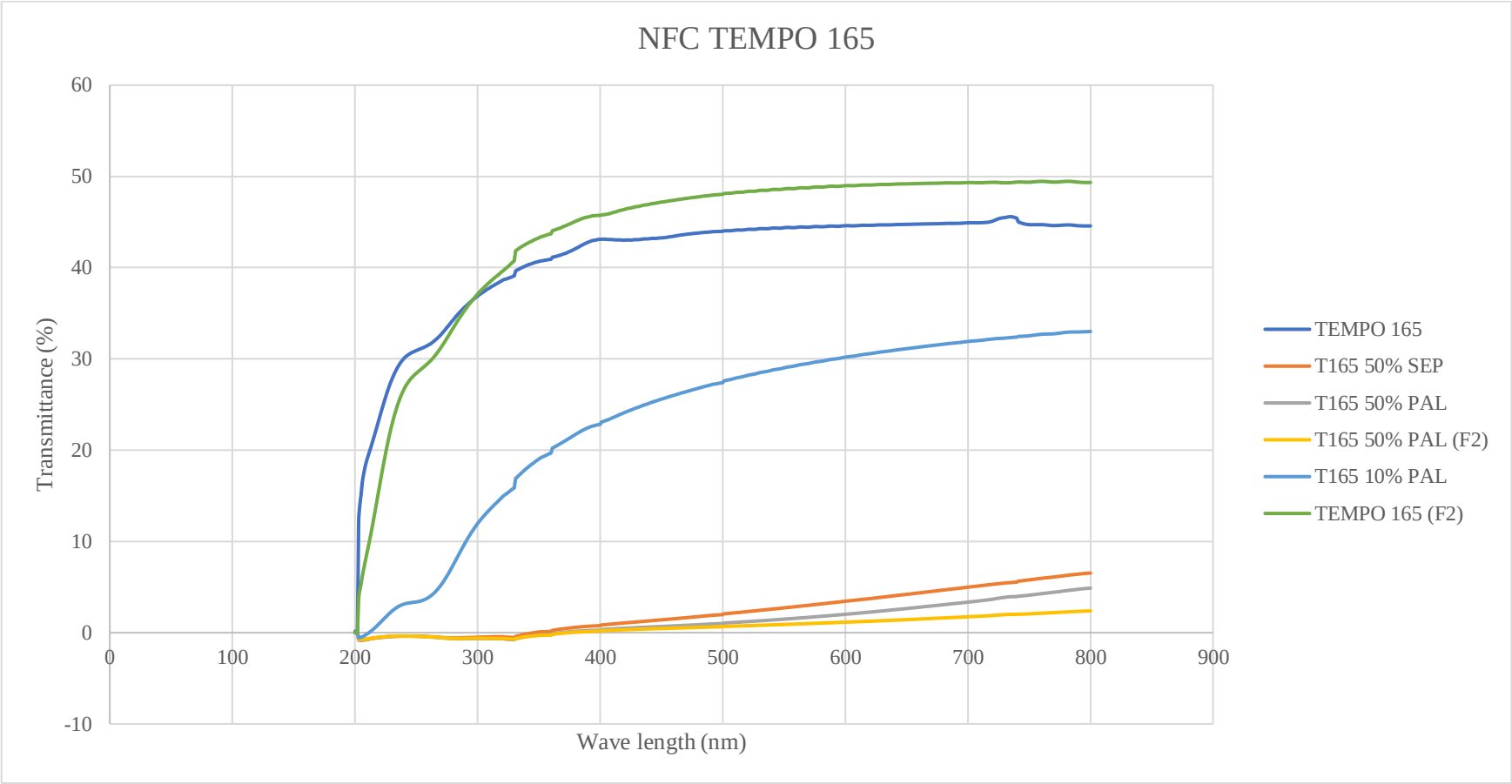

Figure III.5. Light transmittance for NFC TEMPO 165 sample (T165), for films obtained through solvent casting (-) and vacuum filtration (F1 – dried at room temperatures; F2 – dried in the oven at 50ºC).